Towards a standard typology of endogenous landslide seismic sources

F. Provost[1], J.-P. Malet[1], C. Hibert[1], A. Helmstetter[2], M. Radiguet[2], D. Amitrano[2], N. Langet[3], E. Larose[2], C. Abancó[4], M. Hürlimann[5], T. Lebourg[6], C. Levy[7], G. Le Roy[2,8], P. Ulrich[1], M. Vidal[7], and B. Vial[2]

[1]Institut de Physique du Globe de Strasbourg, CNRS UMR 7516, EOST/Université de Strasbourg, 5 rue Descartes, F-67084 Strasbourg Cedex, France.
[2]Univ. Grenoble Alpes, Univ. Savoie Mont Blanc, CNRS, IRD, IFSTTAR, ISTerre, 38000 Grenoble, France.
[3]Norsar, Gunnar Randers Vei 15, NO-2007 Kjeller, Norway.
[4]Geological Hazards Prevention Unit, Institut Cartografic i Geologic de Catalunya, Parc de Montjuïc, SP-08038 Barcelona, Spain.
[5]Departament of Civil and Environmental Engineering, UPC-BarcelonaTECH, C. Jordi Girona 1-3, SP-08034 Barcelona, Spain.
[6]Géosciences Azur, CNRS UMR 7329, OCA/Université de Nice, 250 rue Albert Einstein, F-06905 Sophia-Antipolis Cedex, France.
[7]BRGM, Avenue C. Guillemin, F-45100 Orléans, France.
[8]Géolithe, Crolles, France.

Correspondence: Floriane Provost (f.provost@unistra.fr)

Abstract.

The objective of this work is to propose a standard classification of seismic signals generated by gravitational processes and detected at close distances ($<$ 1 km). We review the studies where seismic instruments have been installed on unstable slopes and discuss the choice of the seismic instruments and the network geometries. Seismic observations acquired at 13 unstable slopes are analyzed in order to construct the proposed typology. The selected slopes are affected by various landslide types (slide, fall, topple, and flow) triggered in various material (from unconsolidated soils to consolidated rocks). We investigate high frequency bands ($>$ 1 Hz) where most of the seismic energy is recorded at the 1 km sensor to source distances. Several signal properties (duration, spectral content and spectrogram shape) are used to describe the sources. We observe that similar gravitational processes generate similar signals at different slopes. Three main classes can be differentiated mainly from the length of the signals, the number of peaks and the duration of the auto-correlation. These classer are the "Slopequake" class corresponds to sources potentially occurring within the landslide body, the "Rockfall" class corresponds to signals generated by rock block impacts, and the "Granular Flow" class corresponds to signals generated by wet or dry debris/rock flows. Sub-classes are further proposed to differentiate specific signals properties (frequency content, resonance, precursory signal). The signal properties of each class and sub-class are described and several signals of the same class recorded at different slopes are presented. Their potential origins are discussed. The typology aims to serve as a standard for further comparisons of the endogenous micro-seismicity recorded on landslides.

1 Introduction

Seismology can be used to record (remotely and in a non-invasive way) ground deformation processes and to measure stress/strain conditions through the hydro-mechanical interactions occurring in the media. Seismology is widely used to understand the physical processes taking place on tectonic faults or volcanoes, to investigate fluid reservoir circulation, and more recently to analyze the dynamics of Earth surface processes such as glaciers (Podolskiy and Walter, 2016), snow avalanches (Leprettre et al., 1996; Sabot et al., 1998; Surin et al., 2000; Lacroix et al., 2011; Pérez-Guillén et al., 2016) and landslides (Deparis et al., 2008; Ekström and Stark, 2013; Gomberg et al., 1995; Rouse et al., 1991). In this manuscript, the term landslide describes a wide variety of processes resulting from the downslope movement of slope-forming materials by falling, toppling, sliding or flowing mechanisms (Hungr et al., 2014). Thus, landslides cover a large range of deformation processes, that can be differentiated in terms of sizes and volumes (smaller than 1 m^3 up to more than 10^7 m^3), in terms of displacement rates (mm.yr^{-1} to m.s^{-1}), and in terms of mobilized material (hard/soft rocks, debris, poorly consolidated soils, and artificial fills).

With the increasing number of seismic sensors deployed worldwide and to the development of automatic seismological processing chains, the construction of landslide catalogs using seismology is now possible, especially at the regional scale (e.g. Switzerland, Hammer et al. (2013); Dammeier et al. (2016); France, Deparis et al. (2008)). However, the forecast of a particular landslide rupture or acceleration is still challenging at the slope scale, which is the focus of this work. In the 1960s, Cadman and Goodman (1967) observed an increase of Acoustic Emissions (AE) generated by slopes tilted towards failure at both laboratory and field scales. AEs are high frequency (10-1000 kHz) body waves generated by the release of strain energy through grain rearrangement (Michlmayr et al., 2012). Further studies confirmed these results for several slopes (Rouse et al., 1991; Smith et al., 2014; Dixon et al., 2015, 2018) where correlations between AE, surface displacement and heavy rainfall were documented. AEs record deep deformation processes before signs of displacement are identifiable at the surface. However, AEs are rapidly attenuated with the distance to the sources. The location of the sensors and the type of waveguide are also critical to capture the slope behavior. Recent developments of Fiber Optic Distributed Acoustic Systems (FO-DAS) offer the opportunity to overcome attenuation limitations and deploy measures over long distances (Michlmayr et al., 2017). More recently, several studies focused on the analysis of the micro-seismicity (MS) observed on unstable slopes. MS studies analyze the seismic waves generated by the release of strain energy in the ground at larger scale than the grain to grain interactions in the frequency range of 1 to 500 Hz. The method offers the opportunity to remotely record the spatial distribution of the deformation through time (McCann and Forster, 1990; BRGM, 1995) and is less sensitive to attenuation than AE methods. Gomberg et al. (1995) installed seismometers on the Slumgullion slow-moving landslide (Colorado, USA) in order to understand the mechanical processes taking place during landslide deformation. Further studies used the same method for several slope configurations (hard/soft rocks, soils, very slow to rapid movements) but also investigated the possible links between the displacement rate and the seismic energy release (Spillmann et al., 2007; Helmstetter and Garambois, 2010; Walter et al., 2012, 2013b; Tonnellier et al., 2013). Helmstetter and Garambois (2010) correlated the seismic response of the Séchilienne rockslide with the surface displacement rate and the rainfall amount. The analysis of the seismic waves generated by landslides allows monitoring spatio-temporal changes of the stress-strain field in the material from the scale of microscopic internal damage (Dixon et al., 2003;

Michlmayr et al., 2012; Smith et al., 2017) to the initiation (e.g. pre-failure) of large ruptures (Amitrano et al., 2005; Yamada et al., 2016b; Poli, 2017; Schöpa et al., 2018). Both the failure and surface processes (e.g. rockfall, debris flow) generate seismic waves. Physical properties (mass, bulk momentum, velocity, trajectory) of the landslide can be inferred from the analysis of the seismic signals (Kanamori et al., 1984; Brodsky et al., 2003; Lacroix and Helmstetter, 2011; Ekström and Stark, 2013; Tang

5 et al., 2015; Hibert et al., 2014a; Levy et al., 2015). On clayey landslides, drops of shear wave velocity have been observed before acceleration episodes. This shear wave variation through time has been documented using noise correlation techniques for laboratory experiments (Mainsant et al., 2012b), and for a few cases in the field at Pont-Bourquin landslide (Switzerland, Mainsant et al. (2012a)), at Harmaliére landslide (France, Bièvre et al. (2017)) and at Just-Tegoborze landslide (Poland, Harba and Pilecki (2017)). Precursory seismic signals are also expected and documented before large failures. Precursory increase in

10 micro-seismic activity (in terms of event rates and/or average amplitudes) has been observed first before the fall of a coastal cliff (Mesnil-Val, France, Amitrano et al. (2005)) and was interpreted as the propagation of a fracture. More recently, repeating events have been detected before the Rausu landslide (Japan, Yamada et al. (2016b)) and the Nuugaatsiaq landslide (Greenland, Poli (2017)). These events are likely associated with the repeated failure of asperities surrounded by aseismic slip, driven by the acceleration of the slope displacement during the nucleation phase of the landslide rupture. Schöpa et al. (2018) recorded

15 harmonic tremors that started 30 min before the failure of the Askja caldera landslide (Iceland) with temporal fluctuations of resonance frequency around 2.5 Hz. This complex tremor signal was interpreted as repeating stick-slip events with very short recurrence times (less than 1 s) producing a continuous signal. However, the characterization of the size of the asperity and the velocity of the ruptures associated to these precursory signals are difficult to invert mostly because of the lack of dense seismic network at close proximity of the slope instability (Schöpa et al., 2018). Therefore, the monitoring of endogenous MS may

20 represent a promising approach especially, with the advent of robust, cheaper and portable seismic sensors and digitizers. It is now possible to install dense sensor networks close to the unstable slopes and record low amplitude signals in broad frequency bands. A wide variety of unstable slopes are currently monitored (i.e. through permanent or campaign installation) with seismic networks of different sizes and instruments (Table 1).

Understanding the possible mechanisms generating these seismic signals needs to be achieved. The discrimination of the

25 endogenous landslide seismic signals is difficult and need to be established. The objective of this paper is thus to propose a typology of the landslide micro-seismic signals recorded in the field. The proposed typology is based on the analysis of observations from 13 monitored sites. The typology includes all the seismic sources recorded at near distances (< 1 km) and in the frequency range of MS studies (1-500 Hz), and generated by landslides 1) developed in hard/soft rocks and soils, 2) characterized by fragile (i.e. rupture) and ductile (i.e. viscous) deformation mechanisms.

30 In our work, we first discuss all the physical processes that occur on landslides and may generate seismic signals. We further present the available seismic sensors, the most commonly used network geometry and the instrumented sites. Then we establish a classification scheme of the landslide seismic signals from relevant signal features based on the analysis of the datasets of 13 sites. We further discuss the perspectives and remaining challenges of monitoring landslide deformation with MS approaches. The seismic signals associated with very large rock/debris avalanches and slides observed at regional distances are out of the

35 scope of this work.

2 Description of landslide endogenous seismic sources

This section describes the possible hydro-mechanical processes observed on landslides and susceptible to generate seismic sources. We present the conditions controlling their occurrences (type of material, topography), their sizes, and their mechanical properties.

2.1 Fracture related sources

The term fracture denominates any discontinuous surface observed in consolidated media and originating from the formation of the rocks (i.e. joint) or the action of tectonic (i.e. schistosity), gravitational or hydraulic loads. In the case of slow-moving landslides, the propagation of the material also creates fractures on the edge and at the base of the moving material. Fractures occur in all type of materials at different scales from grain rupture to metric faults. The term fissure is sometimes used to describe fractures affecting the surface of the ground and for fractures affecting poorly consolidated material. We here include all these surface discontinuities under the general term "fracture". Fractures are generated in three basic modes (I: opening, II: sliding and III: tearing) depending on the movement of the medium on the sides of the fracture plane. They result from either brittle failure of the media or from dessication effects forming polygonal failures during soil drying. On landslides, most of the fractures occur in a tensile mode because of the low tensile toughness of the landslide material and the shallow depth (Stumpf et al., 2013). The formation of fractures can also be generated in depth by progressive degradation of the rock through ground shaking and/or through weathering and long-term damage due to gravitational load. At the base and on the edges of the landslide, the movement is assumed to develop fractures in shear mode, creating sliding surfaces. Shearing on the fracture plane and tensile fracture opening/closing generate seismic signals. Shearing takes place at different scales from earthquakes on tectonic plates to grain friction and generates a variety of seismic signals (Zigone et al., 2011). Unstable regime leads to stick-slip behavior where the stress is regularly suddenly released generating impulsive seismic events. Tremor like signals or isolated impulsive or emergent events are also generated during plate motions. A variety of signals are observed during glacier motion. Deep icequakes are usually associated to basal motion (Winberry et al., 2011; Pratt et al., 2014; Helmstetter et al., 2015a, b; Roeoesli et al., 2016a; Podolskiy and Walter, 2016). Tremor like signals are also recorded during glacier motion (Lipovsky and Dunham, 2016). They are characterized by long duration signals of low amplitudes with no clear phase onsets. They are associated with repetitive stick-slip events on the fracture plane. Tensile fracture opening/closing generate similar signals on glacier at the surface and at depth (Walter et al., 2013a; Helmstetter et al., 2015b; Podolskiy and Walter, 2016). Focal mechanism and location of the source allow to differentiate between tensile and shear mechanism.

2.2 Topple and fall related sources

On vertical to sub-vertical slopes, mass movement occurs as the topple of rock columns or as the free-fall (and possibly bouncing and rolling) of rocky blocks (Hungr et al., 2014). In the case of toppling, the movement starts with a slow rotation of the rock blocks under the effects of water infiltration or ground shaking and ends with the free fall of larger blocks. Rockfalls, during the propagation phase, impact the ground at some location along their trajectory. These impacts generate seismic waves

that can be recorded remotely by seismometers. The range of rockfall volumes can be very large, varying from less than one cubic meter to thousands cubic of meters.

2.3 Mass flow related sources

Mass flows gather different run-out processes of debris or of a mixture of water and debris. They cover a large range of volumes from large rock avalanches of several millions cubic meters to small (hundreds cubic of meters) debris falls and flows (Hungr et al., 2001). They can occur in wet or dry conditions. The contacts of the rock/debris fragments with the bedrock and in the mass flow generate seismic radiations (Suriñach et al., 2001; Burtin et al., 2009; Schneider et al., 2010; Hibert et al., 2011; Abancó et al., 2012; Burtin et al., 2013; Levy et al., 2015; Kean et al.; Vázquez et al., 2016; Hibert et al., 2017b). The seismic signal is hence a combination of grain contacts within the granular flow and of grain to ground surface contacts and hence generate a complex seismic signal.

2.4 Fluid related sources

Hydrological forcing (e.g. precipitation, snow-melt) is one of the most common landslide triggers. The presence of fracture networks, water pipes and the heterogeneity of the rock/soil media result in the development of preferential water flow paths (Richards and Reddy, 2007; Hencher, 2010). These preferential flows induced local saturated area where the increase of pore water pressure may destabilize shallow or deep shear surfaces. In soils, the dissolution of material into finer granular debris creates weak zones prone to collapse either by suffusion (i.e. non cohesive material wash out under mechanical action) or by dispersion (i.e. chemical dissolution of fractured clay soils; Richards, Jones, 1981). In rocks, pipes may develop by erosion. In these saturated fracture networks, hydraulic fracturing can occur creating earthquakes and harmonic tremors related to flow migration in the fractures (Chouet, 1988; Benson et al., 2008; Tary et al., 2014a, b; Derode et al., 2015; Helmstetter et al., 2015b).

3 Landslide seismic investigation

3.1 Sensors used in landslide monitoring

Body and surface mechanical waves may be generated by the sources described in Section 2. Body waves (Primary -P-, Secondary -S-) radiate inside the media. P-waves shake the ground in the same direction they propagate while S-waves shake the ground perpendicularly to their propagation direction. Surface waves only travel along the surface of the ground and their velocity, frequency content and intensity change with the depth of propagation. Acoustic waves can be generated by the conversion of body waves at the surface. These waves travel in the air at a velocity of about 340 m.s^{-1}, slightly varying with temperature and air pressure. Acoustic waves are often generated by anthropogenic or atmospheric sources (e.g., gun shots, explosions, storms...), but can also be generated by rockfalls, debris flows or shallow fracture events. All these mechanical waves are subject to attenuation with the travel distance; the high frequency waves are attenuated faster than the low frequency

waves. The relatively low energy released by the landslide related sources makes the choice of the seismic instruments to deploy very important. Four types of instruments are used to record ground motion for different frequency ranges and sensitivities. For landslide monitoring, Short-Period (SP) seismometers and geophones, Broad-Band (BB) seismometers, accelerometers, and AE sensors are commonly installed in the field.

5   – Broad-Band seismometers are force-balanced sensors with very low corner frequency (< 0.01 Hz) that can record the ground motion with a flat response in a large frequency range [0.01-25] Hz. They require a careful mass calibration during their installation and are sensitive to temperature and pressure variations. They are mostly used to record very weak ground motion and ambient noise;

     – SP-seismometers are passive or force-balanced instruments with high corner frequency (> 1Hz). They measure the

10   velocity of the ground with high sensitivity and a flat response in the [1-100] Hz frequency band. They are recommended for volcanic and glacier monitoring among other applications. They are less sensitive to air temperature and pressure variations and do not require mass calibration. They are hence particularly suitable for landslide monitoring. Geophones are similar to SP-seismometers but usually cover higher frequencies [1-600]Hz with lower sensitivity. They are mainly used for active seismic campaigns but may also be installed for the same purposes as SP-seismometers;

15   – Accelerometers are strong motion sensors able to record high amplitudes and high frequencies seismic waves. They can resolve accelerations in the frequency bands from 0.1 to 10 kHz. The response of the sensor is proportional to ground acceleration for all frequencies (there is no corner frequency). But the noise level is important for low frequencies and the sensitivity is not as good as for velocimeters. They are used to record strong ground motion in particular when installed close to epicenters (< 100 km) of large earthquakes where seismometers usually saturate. For landslide, they are usually

20   used as inclinometers;

     – AE (Acoustic Emission) sensors can record ground vibrations at very high frequencies (10 kHz-10 MHz) and low amplitudes. There are two types of AE sensors: the first type is very sensitive to a narrow frequency band only while the second type is sensitive to a broader frequency band (Michlmayr et al., 2012). In the field, a waveguide is often installed together with AE sensors in order to counteract the attenuation of the signal. They are used in combination with

25   accelerometers for structural monitoring and for laboratory experiments (e.g. loading, shear, flume tests) and can be used on landslide to monitor very low magnitude sources at the grain-to-grain interactions (Dixon et al., 2003; Michlmayr et al., 2012; Smith et al., 2017);

     – in addition, microphones or infrasound sensors can be useful to detect, locate and classify landslides seismic signals (Kogelnig et al., 2014; Schimmel and Hübl, 2016; Helmstetter and Janex, 2017). The detection of acoustic waves and

30   body waves at one point, because they propagate at different velocities, can be used to estimate the distance from the source. The relative amplitude of seismic and acoustic waves can also provide information on the depth of the source, because shallow sources generate more acoustic waves than deeper ones.

It must be noted that AE sensors only record acoustic emissions generated at very high frequencies (> 10kHz) and consequently are very sensitive to attenuation. Indeed, attenuation factor Q is estimated to range between 10^{-2} and 10^1 dB.cm^{-1} (Michlmayr et al., 2012). Even with a waveguide, they must be collocated with the cracks or the sliding surfaces observed on the slope (Dixon et al., 2015). BB, SP seismometers and geophones record seismic signals in the common band of 10^0-10^2 Hz and hence offer a solution to monitor more distant sources. The detection of a seismic sources by MS sensors depends on the seismic energy released by the source, the sensor to the source distance and the attenuation of the media. Installation of MS sensors at the proximity of the geomorphological features of interest (e.g. scarp, faults, sliding surfaces, superficial crack networks, etc.) optimize the detection of the seismic signals generated by those processes but distant sources (> 1 m) can also be recorded by MS sensors. The latter do not need to be co-located with the geomorphological features of interest. After correcting the sensor response, the signals generated by these sensors can be analyzed and compared in their common frequency range. Installation of BB seismometers can complete SP network and enable to investigate the low-frequency signals generated by the slope while geophones are more adapted to explore very high frequency content (> 100 Hz). Dense networks of the latter instruments are recommended to investigate the seismicity induced by landslide deformation while the installation of one unique BB seismometer is enough to investigate the low-frequency radiations of the landslide.

3.2 Network geometry

Several network configurations have been tested in different studies. It must be noted that the network geometry in the case of landslides is constrained by the site configuration. Indeed, the maintenance of seismic sensors may be very challenging when installed on the moving parts of the landslide; therefore, an installation on the most stable parts of the landslide or at its vicinity is often preferred for permanent monitoring (Spillmann et al., 2007; Helmstetter and Garambois, 2010; Walter et al., 2017). During field campaigns, maintenance of sensors installed on the unstable slopes is possible and often realized (Gomberg et al., 2011; Walter et al., 2012; Tonnellier et al., 2013). Therefore, the main challenges for seismic sensor installation at this scale is 1) to locate the sensor at close distance to the sources, 2) to maximize the number of stations and to locate the sensor close to each other to record the same event at different seismic station and 3) minimize the azimuthal gap between the sensors. The number of deployed sensors plays an important in the magnitude of completeness (M$_c$) of the seismic network. While the geometry of the network (i.e. inter-sensor distances, azimuthal gap) mostly control the accuracy of source locations.

Seismic sensors can be deployed in network of single sensors or network of sensor arrays. The difference between seismic network and seismic arrays is related to the distance at which the signals recorded by two sensors can be correlated. In the case of seismic arrays, the distance between the sensors is reduced to maximize the correlation of the signals recorded by each sensor. Otherwise the installation is called a seismic network (Podolskiy and Walter, 2016). Although the inter-sensor distance is often small (< 1 km) in the case of landslide monitoring, decorrelation of the signals is often observed even at small distances due to the complexity of the underground structure especially at high frequencies. The use of the "seismic array" approach in landslide monitoring often refers to specific geometries of collocated sensors (inter-sensors distances < 50 m) organized with a central sensor (often a three-component seismometer) and several satellite sensors (often vertical sensors). This kind of

installation presents many advantages such as enhancing the Signal-to-Noise (SNR) ratio and allowing the computation of the back-azimuth of the source with beam-forming methods.

For the majority of the instrumented landslides, seismic networks are organized with single sensors located on or at close distance of the unstable slopes. The inter-sensors distance and the azimuthal gap are often controlled by the location of easily accessible or stable portions of the slopes. However, specific geometry can be adopted such as (almost) linear geometry. This is particularly the case for the monitoring the propagation of debris flows in stream channels. Dense networks (number of sensors > 50) can also be deployed. In this case the sensors are installed using a grid geometry with regular inter-sensor distances. This kind of installation is probably the most optimal but is currently mostly realized during short acquisition campaigns due to the difficulty to maintain a large number of sensors over long periods (battery, data storage, possible movement of the sensor), especially when installed directly on the unstable zones of landslides. Finally, the installation of sensors at depth (> 1 m) is challenging for landslide and it has currently only been realized on hard-rock slopes (e.g. Randa, Spillmann et al. (2007) or Séchilienne, RESIF/OMIV (2015)). This kind of installation are however very valuable to constrain the depth of the sources.

3.3 MS processing chains

One of the current challenge for landslide MS analysis is the development of dedicated processing chains able to analyze the unconventional seismic signals observed on landslides. The three steps of MS processing are successively: the detection, the classification and the location of the endogenous seismic events. The development of robust and versatile processing chains for analyzing landslide micro-seismicity is challenging because of 1) the low magnitude of the events and the attenuation of the media that results in emergent and low Signal-to-Noise Ratio (SNR) records, 2) the seismic source radiation patterns that may be single centroid source, double couple source or volumetric source, and, 3) the heterogeneity and variation in time (i.e. topography, water table levels, fissures) of the underground structure preventing the construction of precise velocity models and hence, accurate source locations.

First, for detecting automatically or manually the seismic events, the use of spectrograms is common. Spectrograms represent the evolution of the frequency content in time by computing the Fourier Transform on small moving time windows (e.g. < 1 s). Automatic detection is usually carried out with the STA/LTA (Short-Term Average/Long-Term Average) detector (Allen, 1982) applied on the summed energy of the spectrogram (Spillmann et al., 2007; Helmstetter and Garambois, 2010; Tonnellier et al., 2013).

Second, classifying the detected signals can be carried out automatically by discarding exogenous events with simple criteria (i.e. threshold on the signal duration, inter-trace correlation, apparent velocity) but the determination of the threshold to differentiate the class of signals may be difficult. Machine learning algorithms offer nowadays the possibility to automatize and improve this step. Dammeier et al. (2016) developed a Hidden Markov Model (HMM) that can detect automatically in the time series the occurrence of one particular type of events. The success rate of HMM is reasonable and this technique has the advantage of requiring only one single example to scan the time series. The Random Forest algorithm has proven its efficiency for volcanic and landslide signals classification with higher success rate and versatility (Provost et al., 2017a; Hibert et al., 2017c). New signals are successfully classified in multiple pre-defined classes and changes in the source properties may be

detected by change on the uncertainties (Hibert et al., 2017c). It must be noticed that this approach requires a training set with sufficient elements to build the model. Good success rates (i.e. > 85 %) are rapidly reached with 100 elements or more per class. Template-matching filters have also been used in many studies of landslide collapse and glaciers (Allstadt and Malone, 2014; Yamada et al., 2016a; Poli, 2017; Helmstetter et al., 2015a, b; Bièvre et al., 2017; Helmstetter et al., 2017a) in order to detect and classify seismic signals. This method consist in scanning continuous data to search for signals with waveforms similar to template signals. It can detect seismic signals of very small amplitude, smaller than the noise level. Seismic signals are grouped in clusters of similar waveforms, implying similar source locations and focal mechanism.

Finally, the location of the sources is the most challenging step. Common location methods (such as NonLinLoc; Lomax et al. (2000, 2009)) were used in combination to 3D-velocity models for locating impulsive micro-earthquakes occurring at the Randa rockslide (Spillmann et al., 2007). However, a certain number of recorded signals do not exhibit impulsive first arrivals and clear P- and S-waves onsets. For this kind of signal, location methods based on the inter-trace correlation of the surface waves waveform (Lacroix and Helmstetter, 2011) or on the amplitude (Burtin et al., 2016; Walter et al., 2017) are more suitable and easier to automatize. Other methods such as HypoLine (Joswig, 2008) aim at integrating different strategies (i.e. first arrival picking, inter-trace correlation and beam-forming) to locate accurately the epicenter under the control of an operator while (Provost et al., 2018) developed a method combining Amplitude Source Location (ASL) and inter-trace correlation of the first arrivals in an automatic scheme. In most of the studies, the media attenuation field and/or the ground velocity is approximated to an 1D model, and/or do not take into account the topography. Both the complexity of the landslide underground structure and of the recorded seismic signals lead to mis-location of the events that prevents for accurate interpretation of certain sources and leads to false alarms (Walter et al., 2017).

3.4 Instrumented sites

In the last two decades, seismic networks have been installed on several unstable slopes worldwide. Table 1 synthesizes the unstable slopes or debris flow prone catchments instrumented with seismic sensors worldwide. The sites are classified in terms of landslide types (i.e. slide, fall and flow) according to the geomorphological typology of (Cruden and Varnes, 1996). Studies on snow avalanches (Lawrence and Williams, 1976; Kishimura and Izumi, 1997; Sabot et al., 1998; Suriñach et al., 2001; Biescas et al., 2003) are not integrated. Most of the instrumented sites are located in the European Alps (France, Italy and Switzerland). Short-Period (SP) seismometers and Geophones (G) are the most common type of instruments. Their installation and maintenance is easy as they do not require mass calibration in comparison to Broad-band (BB) or long-period (LP) seismometers.

4 Data

Seismic observations from 13 sites are used to propose the typology. The sites are representative of various types of slope movements and lithology (Table 1) with four slides occurring in hard rocks, four slides occurring in soft rocks, three rockfall-prone cliffs occurring in hard and soft rocks and one catchment prone to debris flows. The seismic instruments installed on these

sites are recording the seismicity generated by the slope deformation and are installed either permanently or were acquired during short campaigns (Table 1). The Riou-Bourdoux catchment is the only site where the seismic signals were manually triggered as rock blocks were thrown down the cliff and monitored with cameras, LiDAR and seismic sensors (Hibert et al. (2017a)).

5   The dimension of the unstable slopes range from 60 m × 30 m for the Chamousset cliff to 7 km × 300 m for the St.-Eynard cliff (Table 2). The seismic networks are deployed with various geometry depending on the configuration of the slope, its activity and the duration of the installation. For most of the sites, at least one seismic sensor is deployed on the active zone or very close to (Table 2). The maximal distance to the slope instabilities is 500 m for the St.-Eynard cliff being the largest investigated site of our study.

10   The seismic network geometry of the majority of sites are distributed seismic network where sensors location are regularly installed over the active zone or at its vicinity. In the case of the Rebaixader catchment, the seismic network is installed at the border of the stream channel almost linearly. At the Slumgullion landslide, a dense network has been installed with regular spacing of the seismic sensors. Seismic arrays are installed at the other sites. The geometry of the seismic arrays are triangular shape with the exception of the Séchilienne landslide where an hexagonal shape is used.

15   The instruments are mostly SP seismometers with natural frequencies of 1 Hz to 5 Hz. Fewer geophones and BB seismometers are installed at the sites. The instrument response is corrected for all the dataset. To be consistent with the sensitivity of all the sensors, we do not investigate the data below 1 Hz for BB seismometers and above 100 Hz for SP seismometers and geophones.

     The dataset being analyzed is composed of either published seismic events or published catalogs. The comparison of these 20 events and catalogs enable to compare the signals and to compose the classes of the typology. In the case that no published events or catalogs are available, we analyzed manually the dataset to complete the number of examples for each proposed class (see Section 5 for detailed information).

5   Methodology

The seismic signals recorded at different sites are compared in order to identify common features. Seismic signals result 25 from the convolution of both the wave propagation and of the seismic source mechanism. Consequently, the observation of common signal features in signals recorded at different sites can only be explained by similar source mechanisms. The proposed typology is hence based on the analysis of these common features. We then selected nine signal features in order to quantify the differences and similarities between the different classes. The nine parameters are chosen because they correspond to the criteria used by experts to analyze and classify a seismic signal and also because they can be used in automatic classification 30 algorithms (Fäh and Koch, 2002; Langer et al., 2006; Curilem et al., 2009; Hammer et al., 2012, 2013; Hibert et al., 2014a; Ruano et al., 2014; Maggi et al., 2017; Provost et al., 2017a; Hibert et al., 2017c). They can be computed for any signal types and present a robust framework for future comparison. The selected signal features are:

– the duration of the signal T (expressed in second), computed on the stacked spectrogram of the traces (Helmstetter and Garambois, 2010).

– the dissymetry coefficient of the signal (expressed in percent), computed as:

$$s = \frac{t_m - t_1}{t_2 - t_1} \times 100 \tag{1}$$

with t_1, t_2 and t_m the time of the signal onset, ending and maximum respectively.

– the number of peaks of the signal envelop N_{peaks}, computed as the number of local maximum above 50% of maximal value of the signal envelop. The envelop of the signal is computed as the absolute value of the Hilbert transform of the signal. The envelop is smoothed by a computing the average on a moving window of length: $\delta t = \frac{100}{f_s T}$.

– the duration of the signal auto-correlation, defined as:

$$T_{corr} = \frac{t_c}{T} \tag{2}$$

with,

$$t_c = \max_t (C(t) < 0.2 * max(C)) \tag{3}$$

with C equal to the signal auto-correlation. A_{max} is expressed in percent (%) and represents the duration of the signal correlating with itself. As an example, a signal with a rapid and abrupt change in frequency content will rapidly be uncorrelated (low A_{max}) while a signal with a constant frequency content will have a long auto-correlation (high A_{max}).

– the mean frequency (expressed in Hertz), computed as:

$$F_{mean} = \frac{\sum_{i=1}^{N} PSD(f_i) f_i}{\sum_{i=1}^{N} PSD(f_i)} \tag{4}$$

with the Power Spectral Density (PSD) defined as:

$$PSD(f) = \frac{2|FFT(y)|^2}{N f_s} \tag{5}$$

with f_s and N being the sampling frequency of the signal and the number of samples respectively. The mean frequency is chosen here as it more representative of the signal spectrum energy and less sensitive to noise than the frequency of maximum energy. (Farin et al., 2014).

– the frequency corresponding to the maximal energy of the spectrum F_{max} (expressed in Hertz).

– the frequency bandwidth F_w defined as:

$$F_w = 2\sqrt{\frac{\sum_{i=1}^{N} PSD(f_i) f_i^2}{\sum_{i=1}^{N} PSD(f_i)} - F_{mean}^2} \tag{6}$$

– the minimal frequency of the signal spectrum, computed as:

$$f_{min} = \min_{f}(PSD(f) < 0.2 \times \max(PSD)) \tag{7}$$

– the maximal frequency of the signal spectrum, computed as:

$$f_{max} = \max_{f}(PSD(f) < 0.2 \times \max(PSD)) \tag{8}$$

5   the maximal frequency of the signal spectrum f_{max} (not to be confused with parameter F_{max} defined above).

The signal features are always computed on the trace with the maximal amplitude band-passed in the range [f_c-50] Hz (f_c: natural frequency). This enables to limit the influence of the wave propagation and to compare signals with different sampling frequencies (i.e 120 Hz to 1000 Hz).

Based on already published events and further interpretations, we propose a standard classification of landslide endogenous
10 seismic sources. The non-published datasets are used to investigate the presence of these signals at other sites and to increase the number of examples for different contexts. Numerous signals were analyzed to draw the proposed classification and selected examples are further presented to describe the different classes.

6   Seismic description of the signals - typology

The typology of the signals is based on the duration and the frequency content of the seismic signals. The signals are classified
15 in three main classes: "Slopequake" (SQ), "Rockfall" (RF) and "Granular flow" (GF). For "Slopequake", sub-classes are proposed and discussed based on the frequency content of the signals. Several examples of signals recorded at different sites are presented and the sources are discussed in the corresponding section.

6.1   Rockfall (RF)

Fig 2 displays the seismic waves recorded for a single block fall at the Riou-Bourdoux catchment (French Alps). The block
20 was manually launched in the catchment and recorded with seismic sensors and cameras (Hibert et al., 2017a). The signal is characterized by successive impacts visible both on the waveform and on the spectrograms and lasts around 20 s. The spectral content contains mostly frequencies above 10 Hz but energy below 10 Hz is present for certain impacts (Fig 2a). At closer distance, very high frequencies can be recorded up to 100 Hz (Fig 2a). The auto-correlation remains large over time due to the similitude of the individual impacts signals ($T_{corr} > 10\%$). P- and S- waves are hardly distinguishable on the record and the
25 signals recorded at the seismic sensors are dominated by surface waves (Dammeier et al., 2011; Helmstetter and Garambois, 2010; Hibert et al., 2014a; Levy et al., 2015).

Seismic signals of natural masses detaching from cliffs are presented in Fig 3. They present similar characteristics to the artificially triggered rockfall. Depending on the height of the cliff, the signal lasts between 5 and tens of seconds. The symmetry of the signal ranges from 0 to 80 % depending on the cliff configuration. In general, the most energetic impacts are recorded

at the middle or after the middle of the signal (dissymetry coefficient $> 50\%$). The highest measurable frequency depends on the source-to-sensor distance and can be very high (> 100 Hz). The spectral energy is concentrated in frequencies above 5 Hz, with the largest PSD values (F_{max}) ranging from 20 to 40 Hz. Generally, the Power Spectral Density energy is low below 10-15 Hz with the exception of some case (Fig 5.c) where spectral energy can be observed. The initial falling masses can themselves broke into smaller units during propagation. In this case, the signal does not return to the noise level between the impacts due to developing granular flow (Fig 3b,e,f) leading to the decrease of the duration of the auto-correlation of the signal. When several blocks are falling at the same time, impacts may overlap, so do the peaks of the signals. In certain cases, the first rock free-fall is preceded by a signal that can be associated with the rock detachment. An example of this precursory signal can be observed in Fig 3a,f and in the data reported by Hibert et al. (2011) and Dietze et al. (2017b). The seismic signals of rockfalls contain information on the physics of the process. The seismic energy of rockfall signals is proportional to the volume (Hibert et al., 2014a; Farin et al., 2014). Scaling laws have also been established between seismic energy, momentum, block mass and velocity before impacts (Hibert et al., 2017a). The frequency content is mainly controlled by the block mass. The frequency of the spectral maximum energy decreases when the block mass increases (Farin et al., 2014; Huang et al., 2007; Burtin et al., 2016). If the rockfalls are well isolated, each impact generates impulsive waves. In the case of multiple rockfalls or short distances between the seismic sources and the sensors, the first arrivals may be emergent due to simultaneous arrivals of waves generated by impactors of different sizes impacting the ground at closely spaced time intervals (Levy et al., 2015; Hibert et al., 2014a).

6.2 Granular Flow (GF)

Granular flows are characterized by cigar-shape signals lasting between tens to thousands of seconds. They are subdivided in two classes:

– **Dry granular flow** (Fig 4): These signals are characterized by cigar-shape waveforms of long duration (< 500 s). Due to the absence of water, the source generally propagates over small distances. The duration of auto-correlation is very weak ($T_{corr} \approx 0\%$) and no seismic phase can be distinguished. No distinguishable impacts can be observed in the waveform nor in the spectrogram at the opposite of rockfall signals. The signal onsets is emergent and P- and S- waves are hardly distinguishable and the signal is dominated by surface waves (Deparis et al., 2008; Dammeier et al., 2011; Helmstetter and Garambois, 2010; Hibert et al., 2014a; Levy et al., 2015). The dissymetry coefficient of the signal varies between 30% and 75% and depends on the acceleration and the volume of mass involved in the flow through time (Suriñach et al., 2001; Suriñach et al., 2005; Schneider et al., 2010; Levy et al., 2015; Hibert et al., 2017b). The frequency ranges from 1 to 35 Hz. The maximal frequency of the PSD varies between 5 and 10 Hz and can be larger (up to 20 Hz) when the seismic sensors are located close to the propagation path. The PSD values are significantly low below 3 Hz and incrase rapidly between 3 and 20 Hz.

– **Wet granular flow** (Fig 5): These signals last several thousands of seconds to several hours and correspond to debris flows. They occur during rainfall episodes when fine material and boulders propagates downstream over long distances

(> 500 m). Like dry granular flow, the duration auto-correlation is very weak (T_{corr} =0%) and no seismic phase can be distinguished. The seismic sensors are often installed at very close distance to the flow path so high frequencies up to 100 Hz may be recorded (Abancó et al., 2014; Burtin et al., 2016; Walter et al., 2017). Little energy is present in the low-frequencies (< 10 Hz) depending on the amount of water and the size of the rocky blocks integrated in the flow (Burtin et al., 2016). The signal is emergent and the amplitude variation depends on the mass involved in the flow passing in the vicinity of the sensor. Debris flows are very often divided in a front with the largest boulders and the highest velocity followed by a body and a tail where the sediment concentration and the velocity decreases (Pierson, 1995). The seismic signal amplitude hence increases progressively as the front is passing at the vicinity of the sensor (Abancó et al., 2012; Hürlimann et al., 2014; Burtin et al., 2016; Walter et al., 2017) and decreases progressively, as the front is moving away from the sensor (dissymetry coefficient > 50%). Large spikes and low-frequencies may be observed in the seismic signal corresponding to the front of the debris flow generated by large boulders impacts. The frequency content also changes and, progressively, energy in the lower frequencies decreases (Fig 5.a).

6.3 Slopequake (SQ)

The "Slopequake" class gathers all the seismic signals generated by sources located within the slope at the sub-surface or at depth such as fracture related sources or fluid migration (cf. section 2). Different names have already been proposed for this kind of signals: "slidequakes" (Gomberg et al., 2011), "micro-earthquake" (Helmstetter and Garambois, 2010; Lacroix and Helmstetter, 2011), "quakes" (Tonnellier et al., 2013; Vouillamoz et al., 2017) or "Landslide Micro-Quake (LMQ)" (Brückl, 2017). We here proposed the term "Slopequake" as a general name for these events. They are characterized by short duration (< 10 s) and are sub-divided in two classes "Simple" and "Complex".

6.3.1 Simple Slopequake

"Simple Slopequake" signals are of short (< 2 s) to very short duration (< 1 s) signals. Their main feature is the triangular-shape of the spectrogram with largest amplitudes being recorded in the first part of the signal (dissymetry coefficient < 50%). The first arrivals contain the highest frequencies of the signal and are followed by a decrease of the frequencies. Depending on the frequency content, these signals can be sub-divided into three classes:

- **Low-Frequency Slopequake (LF-SQ)** (Fig 6): The signal lasts between 1 and 5 s. The maximal amplitude of the signal waveform occurs at the beginning or at the center of the signal (15% < dissymetry coefficient < 50%). The waveform presents only one peak and most of the first arrivals are emergent. Phase onsets are difficult to identify. The signals are mostly dominated by surface waves. Consequently, the duration auto-correlation of the signals is large (> 10%). The largest PSD values are observed between 5 and 25 Hz with a mean frequency ranging between 10 and 15 Hz.

- **High-Frequency Slopequake (HF-SQ)** (Fig 7)): The signal lasts between 1 and 5 s. The maximal amplitude of the signal waveform occurs close to the beginning of the signal (dissymetry coefficient < 30%). The waveform presents only one peak and the first arrivals are mainly impulsive. Different phases may be observed (Spillmann et al., 2007;

Lévy et al., 2010): P-arrivals are detected at the beginning of the signal and correspond to the high frequency waves, surface waves are then observed at the time the frequency decreases. However, in general the short sensor to source distance makes difficult the differentiation between the different seismic phases. The auto-correlation these signals is hence lower than for LF-SQ (< 10 %). In most of the cases, the picking of the different waves onset is made difficult because of the sensor-to-source distances and the low frequency sampling. The largest PSD values are observed between 3 and 45 Hz with a mean frequency ranging between 20 and 30 Hz.

- **Hybrid Slopequake (Hybrid-SQ)** (Fig 8)): The signal lasts between 1 and 2 s. It presents the characteristics of the two precedent signals. The brief first arrivals are very impulsive and last less than one second. They are followed by a low-frequency coda similar to the LF-SQ. The maximal amplitude of the signal waveform occurs close to the beginning of the signal (dissymetry coefficient $< 40\%$). The waveform presents only one peak and the first arrivals are impulsive.

These signals are suspected to be associated to boundary or basal sliding (Helmstetter and Garambois, 2010; Gomberg et al., 2011; Walter et al., 2013b; Tonnellier et al., 2013) or fracturing of the slope (Helmstetter and Garambois, 2010; Colombero et al., 2018). Currently, only few studies have proposed inversion of the source tensor (Lévy et al., 2010). To the best of our knowledge, for soft-rock landslides, no source mechanism was modeled. Therefore, it remains difficult to set if the observation of LF- and HF-slopequakes is due to attenuation of the high frequencies with the distance or to the source mechanism. Indeed, the rupture velocity may explain the difference of frequency content and low-frequency earthquakes are observed on tectonic faults (Shelly et al., 2006; Brown et al., 2009; Thomas et al., 2016). They are characterized by low magnitude ($M_w < 2$) and short duration (< 1 s) and constitute at least part of the seismic tremor signal. Therefore, the main assumption for the source of these events are slow rupture (Thomas et al., 2016). Another interpretation for the low frequency quakes dominated by surface waves is crevasse opening (at the surface) as observed in glacier (Deichmann et al., 2000; Mikesell et al., 2012). Colombero et al. (2018) analyzed AE at laboratory scales generated during thermal fracturing. During this experiment, high-frequency AEs are recorded during the heating stage up to the failure of the rock sample and are interpreted as thermal cracking events (Colombero et al., 2018). Low-frequency AEs are recorded during cooling stage (after failure) and are associated to stick-slip events (Colombero et al., 2018).

Hybrid slopequakes are very similar to the events recorded on volcanoes and glaciers with the presence of fluids in conduits or crevasses (Chouet, 1988; Helmstetter et al., 2015b). The sources of these events are assumed to be related to hydro-fracturing. The first high-frequency events corresponding to a brittle failure is followed by water flow into the newly opened cracks (Chouet, 1988; Benson et al., 2008).

The frequency content depends on the sensor to source distance and on the source mechanism. Observation of LF- and HF-SQ may be the signature of on-going processes taking place within the slope instabilities justifying the three proposed classes for simple slopequakes.

6.3.2 Complex Slopequake

The second class of short duration signals has the same general properties as the simple slopequakes but exhibits particular frequency content or precursory events. These additional characteristics change the possible interpretation of the sources. Consequently, these signals are gathered in the class "Complex Slopequake". Three different sub-classes are proposed:

– **Slopequake with precursors** (Fig 9): The third class of short duration signals are similar to the slopequake signals but are preceded by a precursory signal of smaller amplitude (Fig 9). The content of the precursory signal ranges from 5 to 100 Hz depending on the site and is slightly lower than the highest frequency generated by slopequake-like event. The precursory arrival last up to 1.2 s in the presented examples and no clear phases are detected. The frequency content ranges from 5 to 100 Hz but varies significantly at each site. At all sites, the amplitude of the signal is significantly higher for one of the sensor (3 to 50 times higher) when considering vertical traces. The precursory signal is buried in the noise at the sensors with lowest amplitudes and the signal is similar to a LF-slopequake. Such events have never been documented to our knowledge. They are likely to be generated by a strong and local source located at the very close vicinity of one of the sensor (< 10 m) due to the maximal amplitude ($> 10^5$ nm.s^{-1}) and the rapid decrease of the amplitude recorded by the other sensors. Although the signal is similar to certain earthquakes (the precursory signals interpreted as P-waves arrivals and the strong arrivals as surface waves), no earthquake location can explain the signal recorded at the time these events are recorded. Their occurrence in the night time makes a human activity unlikely to be the source. The most probable source would then be the detachment of a single block and its fall in the vicinity to one of the sensor. This kind of precursory signals are observed for some rockfalls (Fig 3.a) and at a the Saint-Martin-le-Vinoux quarry (France; Helmstetter et al. (2011)). At the Saint-Martin-le-Vinoux underground quarry, the duration between the detachment and the signal impact is well correlated to the room height. This interpretation is coherent with the drop of amplitude before the more energetic event at the Chamousset rock column (Fig 9.c) where a progressive decrease of the precursory signal is observed. However, on the other sites (Fig 9.a,.b) such decrease is not present. The one second lasting precursory signal has a constant amplitude and frequency content. Another interpretation could be that these precursory signals are a succession of overlapping slip or fracture events. The interpretation of these signals cannot be established with certainty and further analysis (i.e. location, time of occurrence) and other examples are needed to discriminate the mechanism at work.

– **Tremor-like slopequake** (Fig 10): The last class of short duration signals often last between 1 and 5 seconds (Fig 10). They present a symmetrical waveform (S=50%) with emergent arrivals and slow decrease of the amplitude to the noise level. The frequency ranges from 5 Hz to 25 Hz. High-frequencies may be briefly recorded in certain events (Fig 10.c) . The maximal energy of the PSD corresponds to a frequency of 8 to 13 Hz while the mean energy corresponds to a frequency of 13 to 17 Hz. No seismic phases are identified. The signal is not recorded by all the sensors even when the sensors are organized in small arrays with short inter-sensor distances (< 50 m). Their waveforms and frequency content are similar to the one of the granular flows (Fig 4). Small debris flows have been observed at La Clapière and Super-Sauze landslides and are likely to generate seismic waves; however, small debris flows are not observed at the

Pas de l'Ours landslide when these kinds of seismic signals are recorded. Another possible source mechanisms for such events may also be a very rapid succession (< 1 s) of shear events along the basal or the side bounding strike-slip faults (Hawthorne and Ampuero, 2017). Further investigations are needed to analyze their occurrences over time and their location to confirm one or the other assumptions.

7 Discussion

The proposed typology is summarized in Fig 11. The approach consisted of comparing the datasets of different sites in order to identify the common features of the recorded seismic signals. Three main classes can be differentiated mainly from the length of the signals, the number of peaks and the duration of the auto-correlation. Figure 12 shows more examples of the signal variability for the sites where long seismic catalogs have been recorded (e.g. Aaknes, Chamousset, Séchilienne, Super-Sauze and La Clapière). Only the signals classified as Rockfall, LF- and HF-slopequake are presented because fewer events of the other classes are present in the investigated datasets. The signal features are in good agreement with the defined classes proposed in the present classification (Fig 11). In general, narrow variability is observed on the feature values among the different sites and consequently, the observed features are likely associated to the source mechanism.

However, some variability exist for rockfall events. Indeed, the volume of the blocks and possible breaks control the frequency content and the auto-correlation duration while the height of the scarp will play a significant role in the duration of the event. Depending on the site, rock fall signal can be very similar (e.g. Séchilienne, Fig 12) suggesting a constant source mechanism or very variable (e.g. Super-Sauze, Fig 12). In the case of the Super-Sauze datasets, rockfall are characterized by a lack of energy in high frequencies due in this case to the distance between the seismic network and the scarp. Installation of additional sensors could be the easiest way to get rid of this variability. It must also be noted that, differentiating flow and fall signals may be challenging. Indeed, some of the events are very likely a mix of these two sources. Rockfalls of various blocks may generate granular flows with metric block impacts, both overlapping in the recorded seismic signals. Presence of metric rocks is also observed in debris flow prone torrents; for this type of events, the block impacts within the mass flows are recorded in the seismic signals (Burtin et al., 2016).

Our analysis does not allow at this stage, to conclude whether the frequency content of simple slopequake is associated to source mechanism because complete catalogs differentiating these two classes are not yet available. Colombero et al. (2018) suggested that HF-slopequake are the dominant class of slopequake at the Madonna del Sasso cliff (hard-rock) and were generated by thermal cracking while LF-slopequake associated to frictional sliding are less frequent. Although we did not investigate the whole datasets, no LF-slopequakes were provided at two hard-rock cliffs: Aaknes and Chamousset (Fig 12) while LF-slopequake are recorded at hard-rock slides: La Clapiè re and Séchilienne (Fig 12). This observation seems to confirm the results of Colombero et al. (2018). However, further comparison of the occurrence of the different slopequakes at specific sites in space and time must be done to improve the comprehension of these sources and confirm this statement.

Harmonic signals have also been documented at the Pechgraben and Super-Sauze landslides (Vouillamoz et al., 2017). These signals last from 1 to 5 s and may repeat during minute-lasting sequences. The proposed interpretation includes hydro-

fracturing or repetitive swarms of micro-earthquakes (Vouillamoz et al., 2017) while Gomberg et al. (2011) hypothesized that this kinf of signals were caused by trapped waves along the side-bounding strike-slip fault generated by shear events. In the investigated datasets, similar signals are recorded at the La Clapière and the Aiguilles landslides with a fundamental frequency of 8 ± 1 Hz (Fig 13.b,c). At the Séchilienne landslide, harmonic signals are also detected (Fig 13.d), mostly during the day, with different resonant frequencies between 2 and 12 Hz. Similar signals are observed at the Slumgullion and Super-Sauze but without clear harmonics in the PSD (Fig 13.e,f). The presence of pipes and drains on or in the vicinity of these sites could also explain the origin of these signals justifying that these signals are not included in the Slopequake class as they may not be generated by a slope deformation process. The location of the source, the distribution of the amplitude, the stability of the fundamental frequency and the daily temporal occurrence of the source supports this assumption. Systematic location of these events is needed to determine if they must be integrated or not in the general typology in the case that they are generated by fluid resonance in fractures.

For certain signals, the coda is dominated by resonance frequencies (Fig 3d, Fig 9c) at high frequencies (i.e. 20 and 43Hz), well observed in the spectrogram of the signal. The resonance is not present before the beginning of the signal and hence can not be due to anthropogenic noise (i.e. motors). In the case of Chamousset cliff, Levy et al. (2011) explained the presence of this monochromatic coda by the resonance of the rock column after the occurrence of the rock bridge breakage. At the Super-Sauze, similar resonant coda are observed at the end of certain rockfalls (Figure 4.d). Considering the distance between the main scarp and the seismic arrays (> 300 m) and the absence of large fracture on the scarp, the occurrence of this kind of resonance is very surprising in this case. This signals feature could also result from the wave propagation (i.e. trapped waves).

No long-lasting tremors are presented in this study. Schöpa et al. (2018) recorded a tremor with gliding before the occurrence of the Askja caldera landslide. Similar tremors have been found on the Whillans ice stream in Antarctica during slow slip events (Paul Winberry et al., 2013; Lipovsky and Dunham, 2016), which repeat twice a day with a slip of about 10 cm lasting for about 20 minutes. Therefore, such signals may also occur during the nucleation phase of landslide failure. The question remains unclear if they are not observed because landslide acceleration is aseismic due to high pore fluid pressure (Scholz, 1998) or low normal stress at the sub-surface of the slope.

Difficulties still arise in providing an exhaustive description and interpretation of all the sources from the simple analysis of the proposed signal features, particularly those generating short-duration signals, in particular for the classes discriminated by the frequency content such as LF-SQ and HF-SQ. The ambiguity between propagation effect and source mechanisms prevents further interpretation due to several limitations. Firstly, the location of the sources remain difficult to establish due to the complexity of some of the signals (Gomberg et al., 2011; Lacroix and Helmstetter, 2011; Tonnellier et al., 2013; Provost et al., 2018), the size of the instrumented sites and the complexity of the underground structure that influences the polarisation of the waves (Neuberg et al., 2000) and the sensors (ie. number, location and type: 1C/3C sensor) installed close to the unstable slopes (Godano et al., 2009). The location of the epicenter of most of the events seems coherent with the instabilities deformation field at the surface (Helmstetter and Garambois, 2010; Levy et al., 2011; Walter et al., 2013b; Provost et al., 2018) although resolving dispersion and 3-D heterogeneities of the velocity fields currently prevent to infer the depth of the events and their focal mechanisms. Secondly, a complementary approach to explain the origin of the sources is the analysis of their occurrence

with respect to surface or basal displacement and monitoring of the water content and pore fluid pressures. It requires both exhaustive catalogs of landslide seismicity over long time periods and continuous and distributed datasets of displacements and pore fluid pressures which remain challenging to acquire. Finally, on addition to the characteristics of seismic signals, further information on the sources processes can be obtained from the distribution of the events in time, space and size. Events that occur regularly in time with similar amplitudes are likely associated with the repeated failure of an asperity surrounded by aseismic slip, for instance, at the base of a glacier (Helmstetter et al., 2015a) or of a landslide (Yamada et al., 2016a; Poli, 2017). Signal amplitudes and recurrence times often display progressive variations in time. In contrast, events that are clustered in time and space, with a broad distribution of energies, are more likely associated with the propagation of a fracture (Helmstetter et al., 2015b). The daily distribution of events time can also be helpful to identify anthropogenic sources, that occur mostly during the day. In contrast, natural events are more frequently detected at night, when the noise level is smaller.

Simulations and models are also required to explain the current observations. Indeed, experimental results suggest an increase of acoustic emissions correlated with the increase of the slope velocity (Smith et al., 2017) or an increase of acoustic emission due to the creation of the rupture area (Lockner et al., 1991). Acceleration of pre-existing rupture surface(s) seems to be the mechanism responsible for the seismicity recorded before large rockslide collapse. Yamada et al. (2016a); Poli (2017) argued that the high correlation between the repetitive events could only be explained by stick-slip movement of the locked section(s), while a cracking process would imply a migration of the location of the events and a change in the events waveforms. Schöpa et al. (2018) argued that the presence of gliding frequencies could only be produced by similar sources and hence close location. On the contrary, in the case of the Mesnil-Val column, Senfaute et al. (2009) interpreted the evolution from high frequency to low frequency events as the progressive formation of the rupture surface followed by the final rupture process immediately before the column collapse where both tensile cracks and shearing motion on the created rupture are generated.

8 Conclusions

Over the last decades, numerous studies have recorded seismic signals generated by various types of landslides (i.e. slide, topple, fall and flow), for different kinematic regimes and rock/soil media. These studies demonstrated the added-value of analyzing landslide-induced micro-seismicity to improve our understanding of the mechanisms and to progress in the forecast of landslide evolution.

In this work we propose a review of the endogenous seismic sources generated by the deformation of unstable slopes. A dataset of fourteen slopes is gathered and analyzed. Each of the source is described by nine quantitative features of the recorded seismic signals. Those features provide distinct characteristics for each type of source. A library of relevant signals recorded at relevant site is shared as supplementary material. We propose three main classes "slopequake", "rockfall" and "granular flow" to describe the main type of deformation observed on the slopes. Slopequakes are related to shearing or fracturing processes. This family exhibits the most variability due to the complexity of the sources. These variations are likely to be generated by different source mechanisms. "Rockfall" and "granular flow" classes are associated to mass propagation on the slope surface. They are distinguishable by the number of peaks clearly identified in the seismic signals.

Presently, several descriptions of the seismic sources are proposed for each study case. We believe that a standard typology will allow to discuss and compare seismic signals recorded at many unstable slopes. We encourage future studies to use and possibly enrich the proposed typology. This also requires publication of the datasets and/or catalogs to progress towards a
5 common interpretation. Recently, organizations such as the United States Geological Survey (USGS) or the French Landslide Observatory (OMIV) have started this work (RESIF/OMIV, 2015).

Recent arrival on the market of relatively cheap and autonomous seismometers (eg. ZLand node systems, Raspberry-Shake systems) will allow the deployment of denser seismic networks of 3C sensors. The latter will certainly improve the location accuracy and enable inversion of the focal mechanism of the sources. Moreover, the recent operational applications of Ground-
10 Based SAR (Synthetic Aperture Radar) and terrestrial LiDAR technologies for monitoring purposes shows their relevance to monitor distributed surface displacements. On-going monitoring on several landslides combining those innovative approaches will certainly help to associate SQ events to deformation processes (Dietze et al., 2017b; RESIF/OMIV, 2015; Provost et al., 2017b).

The proposed typology will help to constrain the design of new models to confirm the assumptions on the nature and the
15 properties of the seismic sources. This will be particularly important for 1) explaining the variability of the SQ sources observed at the sites, 2) progressing in the physical understanding of the SQ sources, and 3) ascertaining the spatio-temporal variations of the seismic activity observed at some unstable slopes in relation with their deformation as well as, with external forcings such as intense rainfalls and earthquakes.

Data availability. The library of the endogenous seismic signals recorded at the sites and described in the manuscript is shared as supple-
20 mentary material. The seismic data are shared in the OMIV website: http://www.ano-omiv.cnrs.fr/ressources/library.

Acknowledgements. This work was carried with the support of the French National Research Agency (ANR) through the projects HY-DROSLIDE "Hydrogeophysical Monitoring of Clayey Landslides", SAMCO "Society Adaptation to Mountain Gravitational Hazards in a Global change Context", and TIMES "High-performance Processing Techniques for Mapping and Monitoring Environmental Changes from Massive, Heterogeneous and High Frequency Data Times Series". Additional support by the Open Partial Agreement "Major Hazards" of
25 Council of Europe through the project "Development of Cost-effective Ground-based and Remote Monitoring Systems for Detecting Land-slide Initiation" was available. The continuous seismic data were provided by the Observatoire Multi-disciplinaire des Instabilités de Versant (OMIV) (RESIF/OMIV, 2015). Some seismic signals analyzed were acquired with seismometers belonging to the French national pool of portable seismic instruments SISMOB-RESIF. The authors thank J. Gomberg for the access to the data of the Slumgullion slope, constructive discussions and review of the early version of this paper as well as Nick Rosser and Emma Vann Jones for the access to the data of the North
30 Yorkshire cliff. The authors also thank Naomi Vouillamoz (University of Stuttgart) and Pascal Diot (ONF-RTM) for helping in the data acquisition at, respectively, the Pechgraben site and the Aiguilles-Pas de l'Ours site. The authors gratefully acknowledge Dr. Velio Coviello and Wei-An Chao for their carefull reviews and thorough comments which helped improving the manuscript.

References

Abancó, C., Hürlimann, M., Fritschi, B., Graf, C., and Moya, J.: Transformation of ground vibration signal for debris-flow monitoring and detection in alarm systems, Sensors, 12, 4870–4891, 2012.

Abancó, C., Hürlimann, M., and Moya, J.: Analysis of the ground vibration generated by debris flows and other torrential processes at the Rebaixader monitoring site (Central Pyrenees, Spain), Natural Hazards and Earth System Sciences, 14, 929–943, https://doi.org/10.5194/nhess-14-929-2014, 2014.

Allen, R.: Automatic phase pickers: Their present use and future prospects, Bulletin of the Seismological Society of America, 72, S225–S242, 1982.

Allstadt, K. and Malone, S. D.: Swarms of repeating stick-slip icequakes triggered by snow loading at Mount Rainier volcano, Journal of Geophysical Research: Earth Surface, 119, 1180–1203, https://doi.org/10.1002/2014JF003086, 2014JF003086, 2014.

Amitrano, D., Grasso, J. R., and Senfaute, G.: Seismic precursory patterns before a cliff collapse and critical point phenomena, Geophysical Research Letters, 32, https://doi.org/10.1029/2004GL022270, l08314, 2005.

Amitrano, D., Arattano, M., Chiarle, M., Mortara, G., Occhiena, C., Pirulli, M., and Scavia, C.: Microseismic activity analysis for the study of the rupture mechanisms in unstable rock masses, Natural Hazards and Earth System Sciences, 10, 831–841, https://doi.org/10.5194/nhess-10-831-2010, 2010.

Arattano, M. and Moia, F.: Monitoring the propagation of a debris flow along a torrent, Hydrological Sciences Journal, 44, 811–823, 1999.

Arattano, M., Abancó, C., Coviello, V., and Hürlimann, M.: Processing the ground vibration signal produced by debris flows: the methods of amplitude and impulses compared, Computers & Geosciences, 73, 17 – 27, https://doi.org/https://doi.org/10.1016/j.cageo.2014.08.005, 2014.

Arattano, M., Covellio, V., Abancó, C., Hürlimann, M., and McArdell, B. W.: Methods of Data Processing for Debris Flow Seismic Warning, International Journal of Erosion Control Engineering, 9, 114–121, 2016.

Benson, P. M., Vinciguerra, S., Meredith, P. G., and Young, R. P.: Laboratory Simulation of Volcano Seismicity, Science, 322, 249–252, https://doi.org/10.1126/science.1161927, 2008.

Berti, M., Genevois, R., LaHusen, R., Simoni, A., and Tecca, P.: Debris flow monitoring in the Acquabona watershed on the Dolomites (Italian Alps), Physics and Chemistry of the Earth, Part B: Hydrology, Oceans and Atmosphere, 25, 707–715, 2000.

Bessason, B., Eiríksson, G., Thorarinsson, O., Thórarinsson, A., and Einarsson, S.: Automatic detection of avalanches and debris flows by seismic methods, Journal of Glaciology, 53, 461–472, https://doi.org/10.3189/002214307783258468, 2007.

Biescas, B., Dufour, F., Furdada, G., Khazaradze, G., and Suriñach, E.: Frequency Content Evolution of Snow Avalanche Seismic Signals, Surveys in Geophysics, 24, 447–464, https://doi.org/10.1023/B:GEOP.0000006076.38174.31, 2003.

Bièvre, G., Helmstetter, A., Lacroix, P., Baillet, L., Langlais, M., Vial, B., Voisin, C., Larose, E., and Jongmans, D.: Réactivation du glissement-coulé d'Harmalière (Isère, France), Journées Aléas Gravitaires, Besançon, France, 2017.

Bottelin, P., Levy, C., Baillet, L., Jongmans, D., and Gueguen, P.: Modal and thermal analysis of Les Arches unstable rock column (Vercors massif, French Alps), Geophysical Journal International, 194, pp 849–858, https://doi.org/10.1093/gji/ggt046, 2013a.

Bottelin, P., Jongmans, D., Baillet, L., Lebourg, T., Hantz, D., Levy, C., Roux, O. L., Cadet, H., Lorier, L., Rouiller, J.-D., Turpin, J., and Darras, L.: Spectral Analysis of Prone-to-fall Rock Compartments using Ambient Vibrations, Journal of Environmental and Engineering Geophysics, 18, 205–217, https://doi.org/10.2113/JEEG18.4.205, 2013b.

Bottelin, P., Jongmans, D., Daudon, D., Mathy, A., Helmstetter, A., Bonilla-Sierra, V., Cadet, H., Amitrano, D., Richefeu, V., Lorier, L., Baillet, L., Villard, P., and Donzé, F.: Seismic and mechanical studies of the artificially triggered rockfall at Mount Néron (French Alps, December 2011), Natural Hazards and Earth System Sciences, 14, 3175–3193, https://doi.org/10.5194/nhess-14-3175-2014, 2014.

BRGM: Ecoute acoustique et microsismicité appliquée aux mouvements de terrain. Etat de l'art., Rapport BRGM R38659 , BRGM, document annexe à la PG11., 1995.

5   Brodsky, E. E., Gordeev, E., and Kanamori, H.: Landslide basal friction as measured by seismic waves, Geophysical Research Letters, 30, 2236, https://doi.org/10.1029/2003GL018485, 2003.

Brown, J. R., Beroza, G. C., Ide, S., Ohta, K., Shelly, D. R., Schwartz, S. Y., Rabbel, W., Thorwart, M., and Kao, H.: Deep low-frequency earthquakes in tremor localize to the plate interface in multiple subduction zones, Geophysical Research Letters, 36, https://doi.org/10.1029/2009GL040027, l19306, 2009.

10   Brückl, E.: Large landslides with seismicity, Rock Mechanics and Engineering Volume 4: Excavation, Support and Monitoring, p. 365, 2017.

Brückl, E., Brunner, F. K., Lang, E., Mertl, S., Müller, M., and Stary, U.: The Gradenbach Observatory—monitoring deep-seated gravitational slope deformation by geodetic, hydrological, and seismological methods, Landslides, 10, 815–829, https://doi.org/10.1007/s10346-013-0417-1, 2013.

Burtin, A., Bollinger, L., Cattin, R., Vergne, J., and Nábělek, J. L.: Spatiotemporal sequence of Himalayan debris flow from analysis of

15   high-frequency seismic noise, Journal of Geophysical Research, 114, F04 009, https://doi.org/10.1029/2008JF001198, 2009.

Burtin, A., Hovius, N., Milodowski, D. T., Chen, Y.-G., Wu, Y.-M., Lin, C.-W., Chen, H., Emberson, R., and Leu, P.-L.: Continuous catchment-scale monitoring of geomorphic processes with a 2-D seismological array, Journal of Geophysical Research: Earth Surface, 118, 1956–1974, 2013.

Burtin, A., Hovius, N., McArdell, B. W., Turowski, J. M., and Vergne, J.: Seismic constraints on dynamic links between geomorphic processes

20   and routing of sediment in a steep mountain catchment, Earth Surface Dynamics, 2, 21–33, https://doi.org/10.5194/esurf-2-21-2014, 2014.

Burtin, A., Hovius, N., and Turowski, J. M.: Seismic monitoring of torrential and fluvial processes, Earth Surface Dynamics, 4, 285–307, https://doi.org/10.5194/esurf-4-285-2016, 2016.

Cadman, J. D. and Goodman, R. E.: Landslide Noise, Science, 158, 1182–1184, https://doi.org/10.1126/science.158.3805.1182, 1967.

Chen, Z., Stewart, R., Bland, H., and Thurston, J.: Microseismic activity and location at Turtle Mountain, Alberta, vol. 16, p. 18, Consortium

25   for Research in Elastic Wave Exploration Seismology, CREWES, University of Calgary, Canada, 2005.

Chouet, B.: Resonance of a fluid-driven crack: Radiation properties and implications for the source of long-period events and harmonic tremor, Journal of Geophysical Research: Solid Earth, 93, 4375–4400, https://doi.org/10.1029/JB093iB05p04375, 1988.

Colombero, C., Comina, C., Vinciguerra, S., and Benson, P.: Microseismicity of an unstable rock mass: from field monitoring to laboratory testing, Journal of Geophysical Research: Solid Earth, https://doi.org/10.1002/2017JB014612, 2017JB014612, 2018.

30   Coviello, V., Arattano, M., and Turconi, L.: Detecting torrential processes from a distance with a seismic monitoring network, Natural Hazards, 78, 2055–2080, 2015.

Cruden, D. M. and Varnes, D. J.: Landslide types and processes, in: Landslide investigation and mitigation, edited by Turner, A. K. and Schuster, R. L., Transportation Research Board Special Report, pp. 36–71, National Academy of Sciences, Washington DC, 1996.

Curilem, G., Vergara, J., Fuentealba, G., Acuña, G., and Chacón, M.: Classification of seismic signals at Villarrica volcano (Chile) using

35   neural networks and genetic algorithms, Journal of volcanology and geothermal research, 180, 1–8, 2009.

Dammeier, F., Moore, J. R., Haslinger, F., and Loew, S.: Characterization of alpine rockslides using statistical analysis of seismic signals, Journal of Geophysical Research, 116, F04 024, https://doi.org/10.1029/2011JF002037, 2011.

Dammeier, F., Moore, J. R., Hammer, C., Haslinger, F., and Loew, S.: Automatic detection of alpine rockslides in continuous seismic data using Hidden Markov Models, Journal of Geophysical Research: Earth Surface, 121, 351–371, 2016.

Deichmann, N., Ansorge, J., Scherbaum, F., Aschwanden, A., Bernard, F., and Gudmundsson, G. H.: Evidence for deep icequakes in an Alpine glacier, Annals of Glaciology, 31, 85–90, https://doi.org/10.3189/172756400781820462, 2000.

Deparis, J., Jongmans, D., Cotton, F., Baillet, L., Thouvenot, F., and Hantz, D.: Analysis of Rock-Fall and Rock-Fall Avalanche Seismograms
5   in the French Alps, Bulletin of the Seismological Society of America, 98, 1781–1796, https://doi.org/10.1785/0120070082, 2008.

Derode, B., Guglielmi, Y., De Barros, L., and Cappa, F.: Seismic responses to fluid pressure perturbations in a slipping fault, Geophysical Research Letters, 42, 3197–3203, https://doi.org/10.1002/2015GL063671, 2015GL063671, 2015.

Dietze, M., Mohadjer, S., Turowski, J. M., Ehlers, T. A., and Hovius, N.: Seismic monitoring of small alpine rockfalls – validity, precision and limitations, Earth Surface Dynamics, 5, 653–668, https://doi.org/10.5194/esurf-5-653-2017, 2017a.

10   Dietze, M., Turowski, J. M., Cook, K. L., and Hovius, N.: Spatiotemporal patterns, triggers and anatomies of seismically detected rockfalls, Earth Surface Dynamics, 5, 757–779, https://doi.org/10.5194/esurf-5-757-2017, 2017b.

Dixon, N., Hill, R., and Kavanagh, J.: Acoustic emission monitoring of slope instability: development of an active waveguide system, Proceedings of the Institution of Civil Engineers - Geotechnical Engineering, 156, 83–95, https://doi.org/10.1680/geng.2003.156.2.83, 2003.

15   Dixon, N., Spriggs, M. P., Smith, A., Meldrum, P., and Haslam, E.: Quantification of reactivated landslide behaviour using acoustic emission monitoring, Landslides, 12, 549–560, https://doi.org/10.1007/s10346-014-0491-z, 2015.

Dixon, N., Smith, A., Flint, J. A., Khanna, R., Clark, B., and Andjelkovic, M.: An acoustic emission landslide early warning system for communities in low-income and middle-income countries, Landslides, https://doi.org/10.1007/s10346-018-0977-1, 2018.

Doi, I., Matsuura, S., Shibasaki, T., and Osawa, H.: in: Seismic measurements in a mudstone landslide area, 2015.

20   Ekström, G. and Stark, C. P.: Simple Scaling of Catastrophic Landslide Dynamics, Science, 339, 1416–1419, https://doi.org/10.1126/science.1232887, 2013.

Ekström, G. and Stark, C. P.: Simple scaling of catastrophic landslide dynamics, Science, 339, 1416–1419, https://doi.org/10.1126/science.1232887, 2013.

Fäh, D. and Koch, K.: Discrimination between Earthquakes and Chemical Explosions by Multivariate Statistical Analysis: A Case Study for
25   Switzerland, Bulletin of the Seismological Society of America, 92, 1795–1805, https://doi.org/10.1785/0120010166, 2002.

Farin, M., Mangeney, A., and Roche, O.: Fundamental changes of granular flow dynamics, deposition and erosion processes at high slope angles: insights from laboratory experiments, Journal of Geophysical Research, 119, https://doi.org/10.1002/2013JF002750, 2014.

G., L. R., Amitrano, D., and Helmstetter, A.: Multidisciplinary study of rockfalls in Chartreuse massif, in: Enviroseis, From process to signal - advancing environmental seismology,6-9 June 2017, Ohlstadt, Germany, 2017.

30   Galgaro, A., Tecca, P. R., Genevois, R., and Deganutti, A. M.: Acoustic module of the Acquabona (Italy) debris flow monitoring system, Natural Hazards and Earth System Science, 5, 211–215, 2005.

Godano, M., Regnier, M., Deschamps, A., Bardainne, T., and Gaucher, E.: Focal mechanisms from sparse observations by nonlinear inversion of amplitudes: method and tests on synthetic and real data, Bulletin of the Seismological Society of America, 99, 2243–2264, 2009.

Gomberg, J., Bodin, P., Savage, W., and Jackson, M. E.: Landslide faults and tectonic faults, analogs?: The Slumgullion earthflow, Colorado,
35   Geology, 23, 41–44, https://doi.org/10.1130/0091-7613(1995)023<0041:LFATFA>2.3.CO;2, 1995.

Gomberg, J., Schulz, W., Bodin, P., and Kean, J.: Seismic and geodetic signatures of fault slip at the Slumgullion Landslide Natural Laboratory, Journal of Geophysical Research: Solid Earth, 116, https://doi.org/10.1029/2011JB008304, b09404, 2011.

Hammer, C., Beyreuther, M., and Ohrnberger, M.: A Seismic-Event Spotting System for Volcano Fast-Response Systems, Bulletin of the Seismological Society of America, 102, 948–960, 2012.

Hammer, C., Ohrnberger, M., and Fäh, D.: Classifying seismic waveforms from scratch: a case study in the alpine environment, Geophysical Journal International, 192, 425–439, https://doi.org/10.1093/gji/ggs036, 2013.

Harba, P. and Pilecki, Z.: Assessment of time–spatial changes of shear wave velocities of flysch formation prone to mass movements by seismic interferometry with the use of ambient noise, Landslides, 14, 1225–1233, https://doi.org/10.1007/s10346-016-0779-2, 2017.

Harp, E. L., Reid, M. E., Godt, J. W., DeGraff, J. V., and Gallegos, A. J.: Ferguson rock slide buries California State Highway near Yosemite National Park, Landslides, 5, 331–337, https://doi.org/10.1007/s10346-008-0120-9, 2008.

Hartzell, S., Leeds, A. L., and Jibson, R. W.: Seismic Response of Soft Deposits due to Landslide: The Mission Peak, California, Landslide-Seismic Response of Soft Deposits due to Landslide: The Mission Peak, California, Landslide, Bulletin of the Seismological Society of America, 107, 2008, https://doi.org/10.1785/0120170033, 2017.

Hawthorne, J. and Ampuero, J.-P.: A phase coherence approach to identifying co-located earthquakes and tremor, Geophysical Journal International, 209, 623–642, https://doi.org/10.1093/gji/ggx012, 2017.

Helmstetter, A. and Garambois, S.: Seismic monitoring of Séchilienne rockslide (French Alps): Analysis of seismic signals and their correlation with rainfalls, Journal of Geophysical Research: Earth Surface, 115, https://doi.org/10.1029/2009JF001532, f03016, 2010.

Helmstetter, A. and Janex, G.: Ecoute sismique et acoustique du mouvement de terrain de Séchilienne (Massif de Belledonne), Métrologie en Milieu Extrême, Collection EDYTEM, 2017.

Helmstetter, A., Ménard, G., Hantz, D., Lacroix, P., Thouvenot, F., and Grasso, J.-R.: Etude multidisciplinaire d'un effondrement dans la carrière de ciment de Saint-Martin-le-Vinoux, Journées Aléas Gravitaires, Strasbourg, France, 2011.

Helmstetter, A., Moreau, L., Nicolas, B., Comon, P., and Gay, M.: Intermediate-depth icequakes and harmonic tremor in an Alpine glacier (Glacier d'Argentière, France): Evidence for hydraulic fracturing?, Journal of Geophysical Research: Earth Surface, 120, 402–416, https://doi.org/10.1002/2014JF003289, 2014JF003289, 2015a.

Helmstetter, A., Nicolas, B., Comon, P., and Gay, M.: Basal icequakes recorded beneath an Alpine glacier (Glacier d'Argentière, Mont Blanc, France): Evidence for stick-slip motion?, Journal of Geophysical Research: Earth Surface, 120, 379–401, https://doi.org/10.1002/2014JF003288, 2014JF003288, 2015b.

Helmstetter, A., Larose, E., Baillet, L., and Mayoraz, R.: Repeating quakes detected at Gugla rock-glacier and Alestch rockslide (Valais), 2017a.

Helmstetter, A., Larose, E., Baillet, L., and Mayoraz, R.: Repeating quakes detected at Gugla rock-glacier and Alestch rockslide (Valais), Enviroseis, From process to signal - advancing environmental seismology, Ohlstadt, Germany, 2017b.

Hencher, S. R.: Preferential flow paths through soil and rock and their association with landslides, Hydrological Processes, 24, 1610–1630, https://doi.org/10.1002/hyp.7721, 2010.

Hibert, C., Mangeney, A., Grandjean, G., and Shapiro, N. M.: Slope instabilities in Dolomieu crater, Réunion Island: From seismic signals to rockfall characteristics, Journal of Geophysical Research, 116, F04 032, https://doi.org/10.1029/2011JF002038, 2011.

Hibert, C., Mangeney, A., Grandjean, G., Baillard, C., Rivet, D., Shapiro, N. M., Satriano, C., Maggi, A., Boissier, P., Ferrazzini, V., and Crawford, W.: Automated identification, location, and volume estimation of rockfalls at Piton de la Fournaise volcano, Journal of Geophysical Research: Earth Surface, 119, 1082–1105, https://doi.org/10.1002/2013JF002970, 2014a.

Hibert, C., Malet, J.-P., Bourrier, F., Provost, F., Berger, F., Bornemann, P., Tardif, P., and Mermin, E.: Single-block rockfall dynamics inferred from seismic signal analysis, Earth Surface Dynamics, 5, 283–292, https://doi.org/10.5194/esurf-5-283-2017, 2017a.

Hibert, C., Mangeney, A., Grandjean, G., Peltier, A., DiMuro, A., Shapiro, N. M., Ferrazzini, V., Boissier, P., Durand, V., and Kowalski, P.: Spatio-temporal evolution of rockfall activity from 2007 to 2011 at the Piton de la Fournaise volcano inferred from seismic data, Journal of Volcanology and Geothermal Research, 333-334, 36 – 52, https://doi.org/https://doi.org/10.1016/j.jvolgeores.2017.01.007, 2017b.

Hibert, C., Provost, F., Malet, J.-P., Maggi, A., Stumpf, A., and Ferrazzini, V.: Automatic identification of rockfalls and volcano-tectonic earthquakes at the Piton de la Fournaise volcano using a Random Forest algorithm, Journal of Volcanology and Geothermal Research, 340, 130 – 142, https://doi.org/https://doi.org/10.1016/j.jvolgeores.2017.04.015, 2017c.

Huang, C.-J., Yin, H.-Y., Chen, C.-Y., Yeh, C.-H., and Wang, C.-L.: Ground vibrations produced by rock motions and debris flows, Journal of Geophysical Research: Earth Surface, 112, https://doi.org/10.1029/2005JF000437, f02014, 2007.

Hungr, O., Evans, S. G., Bovis, M. J., and Hutchinson, J. N.: A review of the classification of landslides of the flow type, Environmental and Engineering Geoscience, 7, 221, https://doi.org/10.2113/gseegeosci.7.3.221, 2001.

Hungr, O., Leroueil, S., and Picarelli, L.: The Varnes classification of landslide types, an update, Landslides, 11, 167–194, https://doi.org/10.1007/s10346-013-0436-y, 2014.

Hürlimann, M., Abancó, C., Moya, J., and Vilajosana, I.: Results and experiences gathered at the Rebaixader debris-flow monitoring site, Central Pyrenees, Spain, Landslides, 11, 939–953, https://doi.org/10.1007/s10346-013-0452-y, 2014.

Itakura, Y., Fujii, N., and Sawada, T.: Basic characteristics of ground vibration sensors for the detection of debris flow, Physics and Chemistry of the Earth, Part B: Hydrology, Oceans and Atmosphere, 25, 717–720, 2000.

Joswig, M.: Nanoseismic monitoring fills the gap between microseismic network and passive seismic, First Break, 26, 117–124, 2008.

Kanamori, H., Given, J. W., and Lay, T.: Analysis of seismic body waves excited by the Mount St. Helens eruption of May 18, 1980, Journal of Geophysical Research, 89, 1856–1866, 1984.

Kean, J. W., Coe, J. A., Coviello, V., Smith, J. B., McCoy, S. W., and Arattano, M.: Estimating rates of debris flow entrainment from ground vibrations, Geophysical Research Letters, 42, 6365–6372, https://doi.org/10.1002/2015GL064811.

Kishimura, K. and Izumi, K.: Seismic Signals Induced by Snow Avalanche Flow, Natural Hazards, 15, 89–100, https://doi.org/10.1023/A:1007934815584, 1997.

Kogelnig, A., Hübl, J., Suriñach, E., Vilajosana, I., and McArdell, B. W.: Infrasound produced by debris flow: propagation and frequency content evolution, Natural hazards, 70, 1713–1733, 2014.

Kumagai, H., Palacios, P., Maeda, T., Castillo, D. B., and Nakano, M.: Seismic tracking of lahars using tremor signals, Journal of Volcanology and Geothermal Research, 183, 112 – 121, https://doi.org/https://doi.org/10.1016/j.jvolgeores.2009.03.010, 2009.

Lacroix, P. and Helmstetter, A.: Location of seismic signals associated with microearthquakes and rockfalls on the Séchilienne landslide, French Alps, Bulletin of the Seismological Society of America, 101, 341–353, 2011.

Lacroix, P., Grasso, J., Roulle, J., Giraud, G., Goetz, D., Morin, S., and Helmstetter, A.: Monitoring of snow avalanches using a seismic array: Location, speed estimation, and relationships to meteorological variables, Journal of Geophysical Research: Earth Surface, 117, https://doi.org/10.1029/2011JF002106, 2011.

Langer, H., Falsaperla, S., Powell, T., and Thompson, G.: Automatic classification and a-posteriori analysis of seismic event identification at Soufrière Hills volcano, Montserrat, Journal of Volcanology and Geothermal Research, 153, 1–10, https://doi.org/http://dx.doi.org/10.1016/j.jvolgeores.2005.08.012, 2006.

Larose, E., Carrière, S., Voisin, C., Bottelin, P., Baillet, L., Guéguen, P., Walter, F., Jongmans, D., Guillier, B., Garambois, S., Gimbert, F., and Massey, C.: Environmental seismology: What can we learn on earth surface processes with ambient noise?, Journal of Applied Geophysics, 116, 62 – 74, https://doi.org/https://doi.org/10.1016/j.jappgeo.2015.02.001, 2015.

Larose, E., Bontemps, N., Lacroix, P., and Maquerhua, E. T.: Landslide monitoring in southern Peru: SEG Geoscientists Without Borders® project, in: 2017 SEG International Exposition and Annual Meeting, Society of Exploration Geophysicists, 2017.

Lavigne, F., Thouret, J.-C., Voight, B., Young, K., LaHusen, R., Marso, J., Suwa, H., Sumaryono, A., Sayudi, D., and Dejean, M.: Instrumental lahar monitoring at Merapi Volcano, Central Java, Indonesia, Journal of Volcanology and Geothermal Research, 100, 457–478, 2000.

Lawrence, W. S. and Williams, T. R.: Seismic Signals Associated with Avalanches, Journal of Glaciology, 17, 521–526, https://doi.org/10.3189/S0022143000013782, 1976.

Le Roy, G., Helmstetter, A., Amitrano, D., Guyoton, F., and Roux-Mallouf, R. L.: Seismic characterization of rock falls from detachment to propagation, in: EGU General Assembly, Vienna, Austria, 2018.

Lenti, L., Martino, S., Paciello, A., Prestininzi, A., and Rivellino, S.: Seismometric Monitoring of Hypogeous Failures Due to Slope Deformations, pp. 309–315, Springer Berlin Heidelberg, Berlin, Heidelberg, https://doi.org/10.1007/978-3-642-31445-2_40, 2013.

Leprettre, B. J. P., Navarre, J.-P., and Taillefer, A.: First results from a pre-operational system for automatic detection and recognition of seismic signals associated with avalanches, Journal of Glaciology, 42, 352–363, https://doi.org/10.3189/S0022143000004202, 1996.

Lévy, C., Baillet, L., Jongmans, D., Mourot, P., and Hantz, D.: Dynamic response of the Chamousset rock column (Western Alps, France), Journal of Geophysical Research, 115, F04 043, https://doi.org/10.1029/2009JF001606, 2010.

Levy, C., Jongmans, D., and Baillet, L.: Analysis of seismic signals recorded on a prone-to-fall rock column (Vercors massif, French Alps), Geophysical Journal International, 186, 296–310, https://doi.org/10.1111/j.1365-246X.2011.05046.x, 2011.

Levy, C., Mangeney, A., Bonilla, F., Hibert, C., Calder, E. S., and Smith, P. J.: Friction weakening in granular flows deduced from seismic records at the Soufrière Hills Volcano, Montserrat, Journal of Geophysical Research: Solid Earth, 120, 7536–7557, https://doi.org/10.1002/2015JB012151, 2015JB012151, 2015.

Lipovsky, B. P. and Dunham, E. M.: Tremor during ice-stream stick slip, The Cryosphere, 10, 385–399, https://doi.org/10.5194/tc-10-385-2016, 2016.

Lockner, D., Byerlee, J., Kuksenko, V., Ponomarev, A., and Sidorin, A.: Quasi-static fault growth and shear fracture energy in granite, Nature, 350, 39, 1991.

Lomax, A., Virieux, J., Volant, P., and Berge-Thierry, C.: Probabilistic Earthquake Location in 3D and Layered Models, pp. 101–134, Springer Netherlands, https://doi.org/10.1007/978-94-015-9536-0_5, 2000.

Lomax, A., Michelini, A., and Curtis, A.: Earthquake Location, Direct, Global-Search Methods, pp. 1–33, Springer New York, https://doi.org/10.1007/978-3-642-27737-5_150-2, 2009.

Lotti, A., Saccorotti, G., Fiaschi, A., Matassoni, L., Gigli, G., Pazzi, V., and Casagli, N.: Seismic Monitoring of a Rockslide: The Torgiovannetto Quarry (Central Apennines, Italy), in: Engineering Geology for Society and Territory - Volume 2, edited by Lollino, G., Giordan, D., Crosta, G. B., Corominas, J., Azzam, R., Wasowski, J., and Sciarra, N., pp. 1537–1540, Springer International Publishing, Cham, 2015.

Lube, G., Cronin, S. J., Manville, V., Procter, J. N., Cole, S. E., and Freundt, A.: Energy growth in laharic mass flows, Geology, 40, 475, https://doi.org/10.1130/G32818.1, 2012.

Maggi, A., Ferrazzini, V., Hibert, C., Beauducel, F., Boissier, P., and Amemoutou, A.: Implementation of a multistation approach for automated event classification at Piton de la Fournaise volcano, Seismological Research Letters, 88, https://doi.org/10.1785/0220160189, 2017.

Mainsant, G., Larose, E., Brönnimann, C., Jongmans, D., Michoud, C., and Jaboyedoff, M.: Ambient seismic noise monitoring of a clay landslide: Toward failure prediction, Journal of Geophysical Research: Earth Surface, 117, https://doi.org/10.1029/2011JF002159, f01030, 2012a.

Mainsant, G., Jongmans, D., Chambon, G., Larose, E., and Baillet, L.: Shear-wave velocity as an indicator for rheological changes in clay materials: Lessons from laboratory experiments, Geophysical Research Letters, 39, https://doi.org/10.1029/2012GL053159, l19301, 2012b.

Manconi, A. and Coviello, V.: Evaluation of the Raspberry Shakes seismometers to monitor rock fall activity in alpine environments, in: EGU General Assembly, Vienna, Austria, 2018.

5 Marcial, S., Melosantos, A. A., Hadley, K. C., LaHusen, R. G., and Marso, J. N.: Instrumental lahar monitoring at Mount Pinatubo, Fire and mud: eruptions and lahars of Mount Pinatubo, Philippines, edited by: Newhall, CG and Punongbayan, RS, Washington Press, Seattle, pp. 1015–1022, 1996.

McCann, D. and Forster, A.: Reconnaissance geophysical methods in landslide investigations, Engineering Geology, 29, 59 – 78, https://doi.org/https://doi.org/10.1016/0013-7952(90)90082-C, 1990.

10 Michlmayr, G., Cohen, D., and Or, D.: Sources and characteristics of acoustic emissions from mechanically stressed geologic granular media – A review, Earth-Science Reviews, 112, 97 – 114, https://doi.org/https://doi.org/10.1016/j.earscirev.2012.02.009, 2012.

Michlmayr, G., Chalari, A., Clarke, A., and Or, D.: Fiber-optic high-resolution acoustic emission (AE) monitoring of slope failure, Landslides, 14, 1139–1146, https://doi.org/10.1007/s10346-016-0776-5, 2017.

Mikesell, T. D., van Wijk, K., Haney, M. M., Bradford, J. H., Marshall, H. P., and Harper, J. T.: Monitoring glacier surface seismicity in time
15 and space using Rayleigh waves, Journal of Geophysical Research: Earth Surface, 117, https://doi.org/10.1029/2011JF002259, f02020, 2012.

Navratil, O., Liébault, F., Bellot, H., Theule, J., Travaglini, E., Ravanat, X., Ousset, F., Laigle, D., Segel, V., and Fiquet, M.: High-frequency monitoring of debris flows in the French Alps, in: Proceedings of 12th interpraevent congress, Grenoble, pp. 281–291, 2012.

Neuberg, J., Luckett, R., Baptie, B., and Olsen, K.: Models of tremor and low-frequency earthquake swarms on Montserrat, Journal of
20 Volcanology and Geothermal Research, 101, 83 – 104, https://doi.org/https://doi.org/10.1016/S0377-0273(00)00169-4, 2000.

Norman, E. C., Rosser, N. J., Brain, M. J., Petley, D. N., and Lim, M.: Coastal cliff-top ground motions as proxies for environmental processes, Journal of Geophysical Research: Oceans, 118, 6807–6823, https://doi.org/10.1002/2013JC008963, 2013.

Occhiena, C., Coviello, V., Arattano, M., Chiarle, M., Morra di Cella, U., Pirulli, M., Pogliotti, P., and Scavia, C.: Analysis of microseismic signals and temperature recordings for rock slope stability investigations in high mountain areas, Natural Hazards and Earth System
25 Sciences, 12, 2283–2298, https://doi.org/10.5194/nhess-12-2283-2012, https://www.nat-hazards-earth-syst-sci.net/12/2283/2012/, 2012.

Palis, E., Lebourg, T., Tric, E., Malet, J.-P., and Vidal, M.: Long-term monitoring of a large deep-seated landslide (La Clapiere, South-East French Alps): initial study, Landslides, 14, 155–170, https://doi.org/10.1007/s10346-016-0705-7, 2017.

Paul Winberry, J., Anandakrishnan, S., Wiens, D. A., and Alley, R. B.: Nucleation and seismic tremor associated with the glacial earthquakes of Whillans Ice Stream, Antarctica, Geophysical Research Letters, 40, 312–315, https://doi.org/10.1002/grl.50130, 2013.

30 Pierson, T. C.: Flow characteristics of large eruption-triggered debris flows at snow-clad volcanoes: constraints for debris-flow models, Journal of Volcanology and Geothermal Research, 66, 283 – 294, https://doi.org/https://doi.org/10.1016/0377-0273(94)00070-W, models of Magnetic Processes and Volcanic Eruptions, 1995.

Podolskiy, E. A. and Walter, F.: Cryoseismology, Reviews of Geophysics, 54, 708–758, https://doi.org/10.1002/2016RG000526, 2016RG000526, 2016.

35 Poli, P.: Creep and slip: Seismic precursors to the Nuugaatsiaq landslide (Greenland), Geophysical Research Letters, 44, 8832–8836, https://doi.org/10.1002/2017GL075039, 2017GL075039, 2017.

Pratt, M. J., Winberry, J. P., Wiens, D. A., Anandakrishnan, S., and Alley, R. B.: Seismic and geodetic evidence for grounding-line control of Whillans Ice Stream stick-slip events, Journal of Geophysical Research: Earth Surface, 119, 333–348, https://doi.org/10.1002/2013JF002842, 2014.

Provost, F., Hibert, C., and Malet, J.-P.: Automatic classification of endogenous landslide seismicity using the Random Forest supervised classifier, Geophysical Research Letters, 44, 113–120, https://doi.org/10.1002/2016GL070709, 2016GL070709, 2017a.

5 Provost, F., Malet, J.-P., Hibert, C., and Vergne, J.: Significance and interest of dense seismic arrays for understanding the mechanics of clayey landslides: a test case of 150 nodes at Super-Sauze landslide, in: EGU General Assembly Conference Abstracts, vol. 19, p. 14097, 2017b.

Provost, F., Malet, J.-P., Gance, J., Helmstetter, A., and Doubre, C.: Automatic approach for increasing the location accuracy of slow-moving landslide endogenous seismicity: the APOLoc method, Geophysical Journal International, 2018.

10 Pérez-Guillén, C., Sovilla, B., Suriñach, E., Tapia, M., and Köhler, A.: Deducing avalanche size and flow regimes from seismic measurements, Cold Regions Science and Technology, 121, 25 – 41, https://doi.org/https://doi.org/10.1016/j.coldregions.2015.10.004, 2016.

RESIF/OMIV: RESIF - Réseau Sismologique et géodésique Français / OMIV- French Multidisciplinary Observatory of Versant Instabilities, https://doi.org/http://dx.doi.org/10.15778/RESIF.MT, 2015.

Richards, K. S. and Reddy, K. R.: Critical appraisal of piping phenomena in earth dams, Bulletin of Engineering Geology and the Environ-
15 ment, 66, 381–402, https://doi.org/10.1007/s10064-007-0095-0, 2007.

Roeoesli, C., Helmstetter, A., Walter, F., and Kissling, E.: Meltwater influences on deep stick-slip icequakes near the base of the Greenland Ice Sheet, Journal of Geophysical Research: Earth Surface, 121, 223–240, https://doi.org/10.1002/2015JF003601, 2015JF003601, 2016a.

Roth, M., Dietrich, M., Blikra, L. H., and Lecomte, I.: Seismic Monitoring of the Unstable Rock Slope Site at Áaknes, Norway, pp. 184–192, https://doi.org/10.4133/1.2923645, 2008.

20 Rouse, C., Styles, P., and Wilson, S.: Microseismic emissions from flowslide-type movements in South Wales, Engineering Geology, 31, 91–110, https://doi.org/http://dx.doi.org/10.1016/0013-7952(91)90059-T, 1991.

Ruano, A., Madureira, G., Barros, O., Khosravani, H., Ruano, M., and Ferreira, P.: Seismic detection using support vector machines, Neuro-computing, 135, 273–283, https://doi.org/http://dx.doi.org/10.1016/j.neucom.2013.12.020, 2014.

Sabot, F., Naaim, M., Granada, F., Suriñach, E., Planet, P., and Furdada, G.: Study of avalanche dynamics by seismic methods, image-
25 processing techniques and numerical models, Annals of Glaciology, 26, 319–323, https://doi.org/10.3189/1998AoG26-1-319-323, 1998.

Schimmel, A. and Hübl, J.: Automatic detection of debris flows and debris floods based on a combination of infrasound and seismic signals, Landslides, 13, 1181–1196, https://doi.org/10.1007/s10346-015-0640-z, 2016.

Schneider, D., Bartelt, P., Caplan-Auerbach, J., Christen, M., Huggel, C., and McArdell, B. W.: Insights into rock-ice avalanche dynam-ics by combined analysis of seismic recordings and a numerical avalanche model, Journal of Geophysical Research, 115, F04 026,
30 https://doi.org/10.1029/2010JF001734, 2010.

Scholz, C. H.: Earthquakes and friction laws, Nature, 391, 37, 1998.

Schöpa, A., Chao, W.-A., Lipovsky, B. P., Hovius, N., White, R. S., Green, R. G., and Turowski, J. M.: Dynamics of the Askja caldera July 2014 landslide, Iceland, from seismic signal analysis: precursor, motion and aftermath, Earth Surface Dynamics, 6, 467–485, https://doi.org/10.5194/esurf-6-467-2018, https://www.earth-surf-dynam.net/6/467/2018/, 2018.

35 Senfaute, G., Duperret, A., and Lawrence, J. A.: Micro-seismic precursory cracks prior to rock-fall on coastal chalk cliffs: a case study at Mesnil-Val, Normandie, NW France, Natural Hazards and Earth System Sciences, 9, 1625–1641, 2009.

Shelly, D. R., Beroza, G. C., Ide, S., and Nakamula, S.: Low-frequency earthquakes in Shikoku, Japan, and their relationship to episodic tremor and slip, Nature, 442, 188, 2006.

Smith, A., Dixon, N., Meldrum, P., Haslam, E., and Chambers, J.: Acoustic emission monitoring of a soil slope: Comparisons with continuous deformation measurements, Gétechnique Letters, 4, 255–261, https://doi.org/10.1680/geolett.14.00053, 2014.

Smith, A., Dixon, N., and Fowmes, G. J.: Early detection of first-time slope failures using acoustic emission measurements: large-scale
5   physical modelling, Géotechnique, 67, 138–152, https://doi.org/10.1680/jgeot.15.P.200, 2017.

Spillmann, T., Maurer, H., Green, A. G., Heincke, B., Willenberg, H., and Husen, S.: Microseismic investigation of an unstable mountain slope in the Swiss Alps, Journal of Geophysical Research: Solid Earth, 112, https://doi.org/10.1029/2006JB004723, b07301, 2007.

Stumpf, A., Malet, J.-P., Kerle, N., Niethammer, U., and Rothmund, S.: Image-based mapping of surface fissures for the investigation of landslide dynamics, Geomorphology, 186, 12–27, https://doi.org/http://dx.doi.org/10.1016/j.geomorph.2012.12.010, 2013.

10   Suriñach, E., Furdada, G., Sabot, F., Biesca, B., and Vilaplana, J. M.: On the characterization of seismic signals generated by snow avalanches for monitoring purposes, Annals of Glaciology, 32, 268–274, https://doi.org/10.3189/172756401781819634, 2001.

Suriñach, E., Vilajosana, I., Khazaradze, G., Biescas, B., Furdada, G., and Vilaplana, J. M.: Seismic detection and characterization of land-slides and other mass movements, Natural Hazards and Earth System Sciences, 5, 791–798, https://doi.org/10.5194/nhess-5-791-2005, 2005.

15   Surin, E., Sabot, F., Furdada, G., Vilaplana, J., et al.: Study of seismic signals of artificially released snow avalanches for monitoring purposes, Physics and Chemistry of the Earth, Part B: Hydrology, Oceans and Atmosphere, 25, 721–727, 2000.

Suwa, H., Okano, K., and Kanno, T.: Behavior of debris flows monitored on test slopes of Kamikamihorizawa Creek, Mount Yakedake, Japan, International Journal of Erosion Control Engineering, 2, 33–45, 2009.

Tang, C., Li, L., Xu, N., and Ma, K.: Microseismic monitoring and numerical simulation on the stability of high-
20   steep rock slopes in hydropower engineering, Journal of Rock Mechanics and Geotechnical Engineering, 7, 493 – 508, https://doi.org/https://doi.org/10.1016/j.jrmge.2015.06.010, 2015.

Tary, J.-B., Van der Baan, M., and Eaton, D. W.: Interpretation of resonance frequencies recorded during hydraulic fracturing treatments, Journal of Geophysical Research: Solid Earth, 119, 1295–1315, https://doi.org/10.1002/2013JB010904, 2014a.

Tary, J.-B., Van der Baan, M., Sutherland, B., and Eaton, D. W.: Characteristics of fluid-induced resonances observed during microseismic
25   monitoring, Journal of Geophysical Research: Solid Earth, 119, 8207–8222, https://doi.org/10.1002/2014JB011263, 2014b.

Thomas, A. M., Beroza, G. C., and Shelly, D. R.: Constraints on the source parameters of low-frequency earthquakes on the San Andreas Fault, Geophysical Research Letters, 43, 1464–1471, https://doi.org/10.1002/2015GL067173, 2015GL067173, 2016.

Tonnellier, A., Helmstetter, A., Malet, J.-P., Schmittbuhl, J., Corsini, A., and Joswig, M.: Seismic monitoring of soft-rock landslides: the Super-Sauze and Valoria case studies, Geophysical Journal International, 193, 1515–1536, 2013.

30   Vázquez, R., Suriñach, E., Capra, L., Arámbula-Mendoza, R., and Reyes-Dávila, G.: Seismic characterisation of lahars at Volcán de Colima, Mexico, Bulletin of Volcanology, 78, 8, https://doi.org/10.1007/s00445-016-1004-9, 2016.

Vilajosana, I., Suriñach, E., Abellán, A., Khazaradze, G., Garcia, D., and Llosa, J.: Rockfall induced seismic signals: case study in Montserrat, Catalonia, Natural Hazards and Earth System Sciences, 8, 805–812, https://doi.org/10.5194/nhess-8-805-2008, 2008.

Voisin, C., Garambois, S., Larose, E., and Massey, C.: Seismic noise correlations and monitoring of the Utiku (New-Zealand) landslide, in:
35   EGU General Assembly Conference Abstracts, vol. 15 of *EGU General Assembly Conference Abstracts*, pp. EGU2013–5406, 2013.

Vouillamoz, N., Rothmund, S., and Joswig, M.: Characterizing the complexity of seismic signals at slow-moving clay-rich debris slides: The Super-Sauze (Southeastern France) and Pechgraben (Upper Austria) case studies, Earth Surface Dynamics Discussions, 2017, 1–34, https://doi.org/10.5194/esurf-2017-65, 2017.

Walter, F., Dalban Canassy, P., Husen, S., and Clinton, J. F.: Deep icequakes: What happens at the base of Alpine glaciers?, Journal of Geophysical Research: Earth Surface, 118, 1720–1728, https://doi.org/10.1002/jgrf.20124, 2013a.

5 Walter, F., Burtin, A., McArdell, B. W., Hovius, N., Weder, B., and Turowski, J. M.: Testing seismic amplitude source location for fast debris-flow detection at Illgraben, Switzerland, Natural Hazards and Earth System Sciences, 17, 939–955, https://doi.org/10.5194/nhess-17-939-2017, 2017.

Walter, M., Walser, M., and Joswig, M.: Mapping Rainfall-Triggered Slidequakes and Seismic Landslide-Volume Estimation at Heumoes SlopeAll rights reserved. No part of this periodical may be reproduced or transmitted in any form or by any means, electronic or mechani-

10 cal, including photocopying, recording, or any information storage and retrieval system, without permission in writing from the publisher, Vadose Zone Journal, 10, 487–495, 2011.

Walter, M., Arnhardt, C., and Joswig, M.: Seismic monitoring of rockfalls, slide quakes, and fissure development at the Super-Sauze mudslide, French Alps, Engineering Geology, 128, 12–22, https://doi.org/http://dx.doi.org/10.1016/j.enggeo.2011.11.002, 2012.

Walter, M., Gomberg, J., Schulz, W., Bodin, P., and Joswig, M.: Slidequake Generation versus Viscous Creep at Softrock-landslides: Syn-

15 opsis of Three Different Scenarios at Slumgullion Landslide, Heumoes Slope, and Super-Sauze Mudslide, Journal of Environmental & Engineering Geophysics, 18, 269–280, https://doi.org/10.2113/JEEG18.4.269, 2013b.

Winberry, J. P., Anandakrishnan, S., Wiens, D. A., Alley, R. B., and Christianson, K.: Dynamics of stick-slip motion, Whillans Ice Stream, Antarctica, Earth and Planetary Science Letters, 305, 283 – 289, https://doi.org/https://doi.org/10.1016/j.epsl.2011.02.052, 2011.

Worni, R., Huggel, C., Stoffel, M., and Pulgarín, B.: Challenges of modeling current very large lahars at Nevado del Huila Volcano, Colombia,

20 Bulletin of Volcanology, 74, 309–324, https://doi.org/10.1007/s00445-011-0522-8, https://doi.org/10.1007/s00445-011-0522-8, 2012.

Yamada, M., Mangeney, A., Matsushi, Y., and Moretti, L.: Estimation of dynamic friction of the Akatani landslide from seismic waveform inversion and numerical simulation, Geophysical Journal International, 206, 1479–1486, https://doi.org/10.1093/gji/ggw216, 2016a.

Yamada, M., Mori, J., and Matsushi, Y.: Possible stick-slip behavior before the Rausu landslide inferred from repeating seismic events, Geophysical Research Letters, 43, 9038–9044, https://doi.org/10.1002/2016GL069288, 2016GL069288, 2016b.

25 Yin, H., Huang, C., Chen, C., Fang, Y., Lee, B., and Chou, T.: The present development of debris flow monitoring technology in Taiwan—a case study presentation, in: 5th International Conference on Debris-Flow Hazards Mitigation: Mechanics, Prediction and Assessment, edited by: Genevois, R., Hamilton, DL, and Prestininzi, A., Casa Editrice Universita La Sapienza, Roma, pp. 623–631, 2011.

Zigone, D., Voisin, C., Larose, E., Renard, F., and Campillo, M.: Slip acceleration generates seismic tremor like signals in friction experiments, Geophysical Research Letters, 38, https://doi.org/10.1029/2010GL045603, l01315, 2011.

30 Zimmer, V. L. and Sitar, N.: Detection and location of rock falls using seismic and infrasound sensors, Engineering Geology, 193, 49–60, 2015.

Zobin, V. M., Plascencia, I., Reyes, G., and Navarro, C.: The characteristics of seismic signals produced by lahars and pyroclastic flows: Volcán de Colima, México, Journal of Volcanology and Geothermal Research, 179, 157–167, 2009.
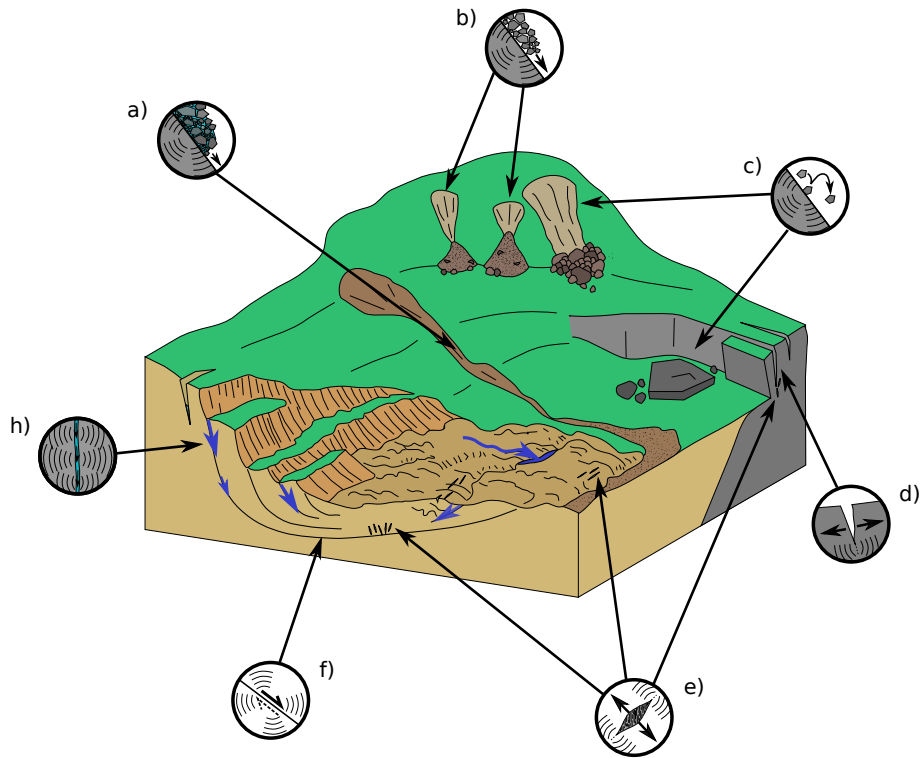
Figure 1. Conceptual scheme of the landslide endogenous seismic sources with a) wet granular flow, b) dry granular flow, c) rockfall, d) tensile fracture opening, e) tensile cracks opening, f) shearing and h) fluid migration in fracture.

Table 1: Table of the instrumented sites. The bolded names correspond to the sites investigated in the present paper to establish the typology.

Number	Site	Location	Type	Material	Sensor	Duration	Reference/Research Group
1	Randa	Switzerland	Slide	Hard rock	G	SC	Spillmann et al. (2007)
2	**Séchilienne**	France	Slide	Hard rock	G, SP	P	RESIF/OMIV (2015); Helmstetter and Garambois (2010); Lacroix and Helmstetter (2011)
3	**La Clapière**	France	Slide	Hard rock	SP(?)	P	RESIF/OMIV (2015); Palis et al. (2017)
4	**Aaknes**	Norway	Slide	Hard rock	G,BB	P	Roth et al. (2008)
5	Peschiera Spring	Italy	Slide	Hard rock	A	SC	Lenti et al. (2013)
6	Gradenbach	Austria	Slide	Hard rock	SP	P(?)	Brückl et al. (2013)
7	Alestch-Moosfluh	Switzerland	Slide	Hard rock	BB	P	Helmstetter et al. (2017b); Manconi and Coviello (2018)
8	Assisi	Italy	Slide	Hard rock	SP	SC	Lotti et al. (2015)
9	Akatami landslide	Japan	Slide	Hard rock	(?)	(?)	-
10	Akkeshi landslide	Japan	Slide	Hard rock	SP	P	Doi et al. (2015)
11	Rausu landslide	Japan	Slide	Hard rock	BB	P	Yamada et al. (2016a)
12	Fergurson slide / Mercel River	USA / California	Slide	Hard rock	(?)	(?)	Harp et al. (2008)
13	Turtle Mountain - Frank slide	Canada	Slide	Hard rock	G	P	Chen et al. (2005)
14	**Aiguilles-Pas de l'Ours**	France	Slide	Soft rock / Earth	BB	SC	RESIF/OMIV (2015)
15	Harmalière	France	Slide	Soft-rock	SP,BB	P	Bièvre et al. (2017)
16	Utiku	New Zealand	Slide	Soft rock / Earth	(?)	P	Voisin et al. (2013)
17	Villerville	France	Slide	Soft rock / Mud	BB	SC,P	RESIF/OMIV (2015)
18	**Super-Sauze**	France	Slide	Soft rock / Mud	SP	P, RC	RESIF/OMIV (2015); Walter et al. (2012); Tonnellier et al. (2013); Vouillamoz et al. (2017)
19	**Pont Bourquin**	Switzerland	Slide	Mud	SP(?)	P	Mainsant et al. (2012a); Larose et al. (2015)
20	Valoria	Italy	Slide	Mud	SP	SC	Tonnellier et al. (2013)
21	**Pechgraben**	Austria	Slide	Mud	SP,BB	RC	Vouillamoz et al. (2017)
22	US highway 50, CA	USA	Slide	Earth	G	P	USGS (https://landslides.usgs.gov/monitoring/)

Number	Site	Location	Type	Material	Sensor	Duration	Reference/Research Group
23	**Slumgullion**	USA	Slide	Earth	G	RC	Gomberg et al. (1995, 2011)
24	Millcoma Meander, Oregon	USA	Slide	Earth	G	P	USGS (https://landslides.usgs.gov/monitoring/)
25	Xishancun	China	Slide	Earth	BB	SC	-
26	Chambon Tunnel	France	Slide	Earth	SP	P	
27	Maca	Peru	Slide	Soft rock / Earth	SP	P(?)	Larose et al. (2017)
28	Heumoes	Germany	Slide	Soft rock / Earth	SP	RC	Walter et al. (2011)
29	Mission Peak landslide	USA / California	Slide	Soft rock / Earth	BB	P	Hartzell et al. (2017)
30	Char d'Osset	France	Slide, Fall	Soft rock / Mud			
31	Mesnil-Val	France	Fall	Hard rock	G	SC	Amitrano et al. (2005); Senfaute et al. (2009)
32	North Yorkshire coast	United Kingdom	Fall	Hard rock	BB	P	Norman et al. (2013)
33	Matterhorn	Italy	Fall	Hard rock	G	RC	Amitrano et al. (2010); Occhiena et al. (2012)
34	Madonna del sasso	Italy	Fall	Hard rock	SP	P(?)	Colombero et al. (2018)
35	**Chamousset**	France	Fall	Hard rock	SH	RC	Lévy et al. (2010); Bottelin et al. (2013b)
36	Mont-Granier	France	Fall	Hard rock	BB	P	-
37	Les Arches	France	Fall	Hard rock	SP	P(?)	Bottelin et al. (2013a, b)
38	La Praz	France	Fall	Hard rock	SP	P(?)	Bottelin et al. (2013b)
39	Rubi	France	Fall	Hard rock	SP	P(?)	Bottelin et al. (2013b)
40	La Suche	Switzerland	Fall	Hard rock	SP	P(?)	Bottelin et al. (2013b)
41	**St. Eynard**	France	Fall	Hard rock	SP	P(?)	G. et al. (2017); Le Roy et al. (2018)
42	Cap d'Ailly	France	Fall	Hard rock			-
43	Lauterbrunnen valley	Switzerland	Fall	Hard rock	BB	SC	Dietze et al. (2017a, b)
44	Three Brothers	USA	Fall	Hard rock	SP	SC	Zimmer and Sitar (2015)
45	Mount Néron	France	Fall (triggered)	Hard rock	BB	SC	Bottelin et al. (2014)
46	**Riou Bourdoux**	France	Fall (triggered)	Hard rock	SP,BB	SC	Hibert et al. (2017a)
47	Montserrat	Spain	Fall (triggered)	Hard rock	SP	SC	Vilajosana et al. (2008)
48	**Piton de la Fournaise**	France	Fall, Flow	Volcanic rock	BB	P	OPVF/IPGP, Hibert et al. (2011, 2014a); Levy et al. (2015); Hibert et al. (2017c)
49	Bolungavík - Oshlíðslope	Iceland	Fall, Flow	Hard rock	A	P	Bessason et al. (2007)
50	**Rebaixader**	Spain	Flow	Debris	G	P	Abancó et al. (2012, 2014); Hürlimann et al. (2014); Arattano et al. (2014)
51	Manival torrent	France	Flow	Debris	G	P	Navratil et al. (2012)
52	Réal torrent	France	Flow	Debris	G	P	Navratil et al. (2012); Coviello et al. (2015)
53	Marderello torrent	Italy	Flow	Debris	G	P	Arattano et al. (2016)
54	Acquabona torrent	Italy	Flow	Debris	G	P(?)	Berti et al. (2000); Galgaro et al. (2005)
55	Moscardo torrent	Italy	Flow	Debris	SP	P	Arattano and Moia (1999)
56	Gadria torrent	Italy	Flow	Debris	G	P	Arattano et al. (2016)
57	Mt. Yakedake volcano - Kamikamihorizawa Creek	Japan	Flow	Debris			Suwa et al. (2009)
58	Lattenbach torrent	Austria	Flow	Debris	G	P(?)	Schimmel and Hübl (2016); Kogelnig et al. (2014)
59	Illgraben torrent	Switzerland	Flow	Debris	G	P	Burtin et al. (2014); Walter et al. (2017)
60	Farstrine torrent	Austria	Flow	Debris	G	P(?)	Schimmel and Hübl (2016)
61	Wartschenbach torrent	Austria	Flow	Debris	G	P(?)	Schimmel and Hübl (2016)
62	Dristenau torrent	Austria	Flow	Debris	G	P(?)	Schimmel and Hübl (2016)
63	Shenmu creek	Taiwan	Flow	Debris	G	P	Yin et al. (2011)
64	Ai-Yu-Zi creek	Taiwan	Flow	Debris	G	P	Huang et al. (2007)
65	Fong-Ciou creek	Taiwan	Flow	Debris	G	P	Huang et al. (2007)
66	Chenyoulan creek	Taiwan	Flow	Debris	G	SC	Burtin et al. (2013)
67	Mt. Sakurajima Volcano - Nojiri Torrent	Japan	Flow	Debris	G	P	Itakura et al. (2000)
68	Mount Pinatubo	Philippines	Flow	Debris	G	P	Marcial et al. (1996)
69	Colima volcano	Mexico	Flow	Debris	LP	P	Zobin et al. (2009); Vázquez et al. (2016)
70	Merapi volcano	Indonesia	Flow	Debris	G	P	Lavigne et al. (2000)
71	Nevado del Huila volcano	Colombia	Flow	Debris	G	P?	Worni et al. (2012)
72	Cotopaxi volcano	Ecuador	Flow	Debris	BB	P	Kumagai et al. (2009)
73	Mount Ruapehu	New-Zeland	Flow	Debris	BB	P	Lube et al. (2012)
74	Sawatch Range, Colorado	USA	Flow	Debris	G	P	Kean et al.

G: Geophone (f = [0.1-10] kHz); SP: Short-Period (f = [0.1-100] Hz); BB: Broad-Band (f = [10^{-2}-100] Hz); A: Accelerometer;

P: Permanent monitoring; RC: Repetitive Campaigns; SC: Single Campaign.

OPVF/IPGP: Volcanological Observatory of the Piton de la Fournaise / Institut de Physique du Globe de Paris.

USGS: United States Geological Survey.
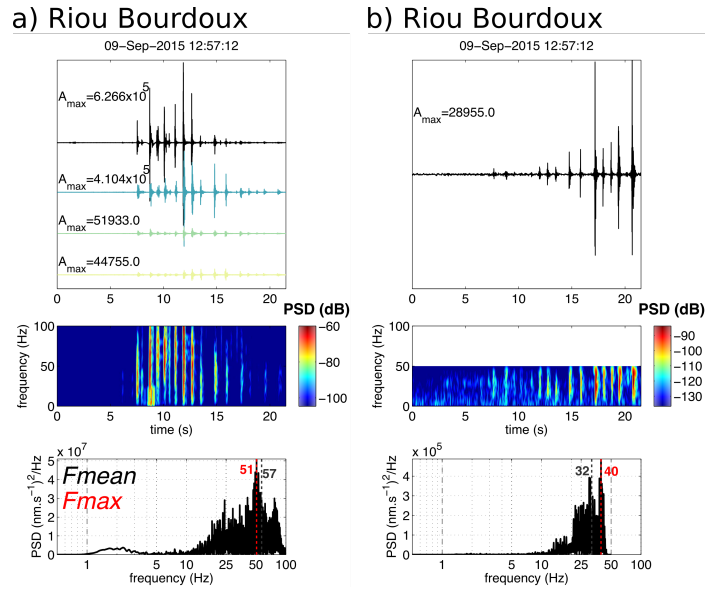
Figure 2. Example of one controlled rockfall (mass= 430kg) at the Riou-Bourdoux catchment (Hibert et al., 2017a) recorded by SP seismometer located at 50 m of the rock departure (left) and recorded by BB seismometer near the rock arrival (right). The waveforms of the vertical traces are plotted on the upper part of the figure. The amplitude are normalized on the trace with the maximal amplitude (black), the signal recorded by the other sensors (when available) are represented in color below. The maximal amplitudes (A_{max}) of all the traces are plotted on the sub-plot in $nm.s^{-1}$. The spectrogram is plotted on the middle part of the figure and normalized to the maximal energy. The lower part of the figure represents the PSD of the most energetic trace and the frequency corresponding to the maximum and the mean of the PSD are plotted in red and gray respectively.
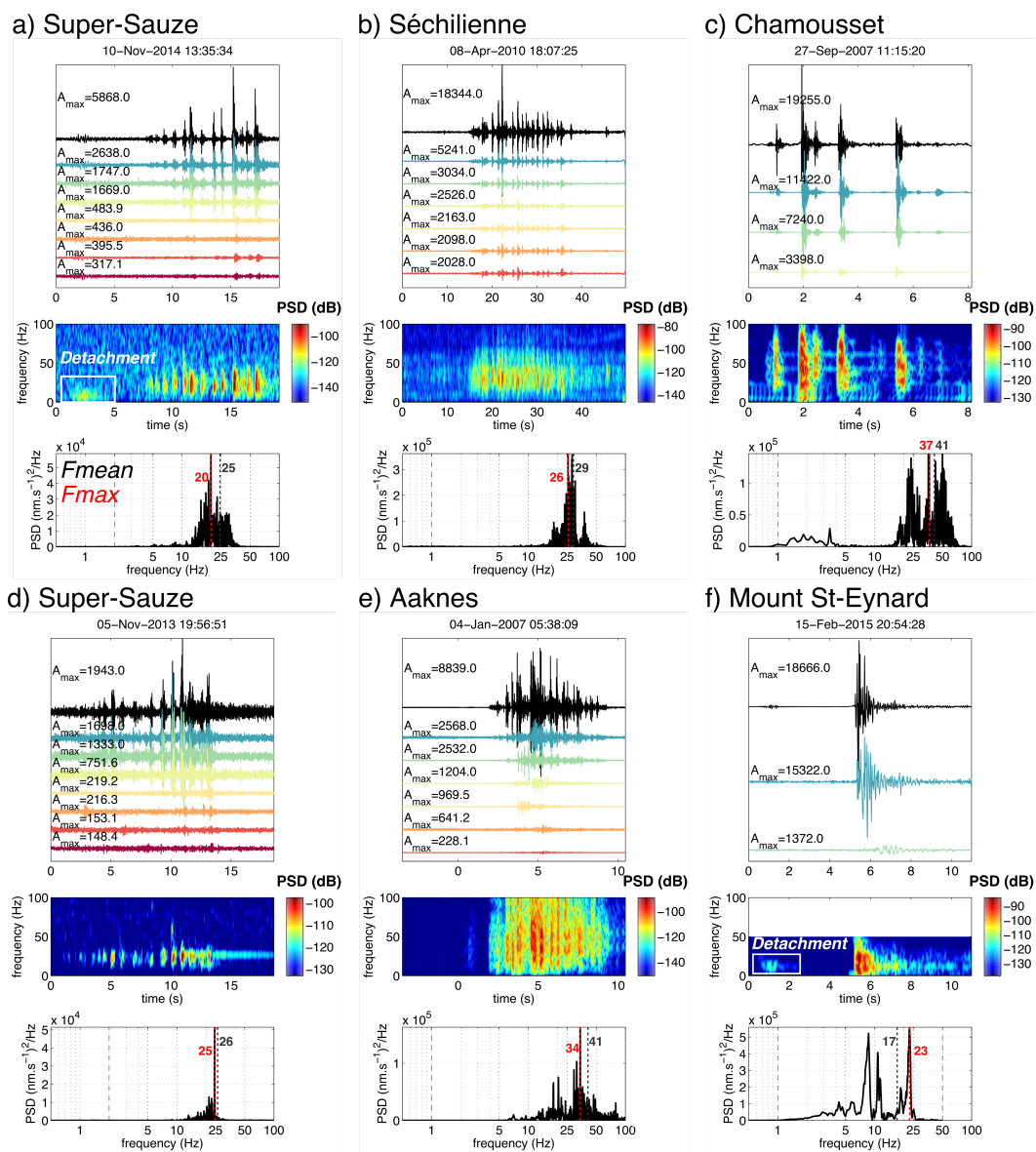
Figure 3. Rockfall events recorded at a) and d) Super-Sauze (France) (Provost et al., 2017a), b) at the Séchilienne (France, Helmstetter et al. (2011); RESIF/OMIV (2015)), c) Chamousset (Levy et al., 2011), e) Aaknes and f) Mount Saint-Eynard slopes (Le Roy et al., 2018). See Fig. 2 for description of the figure.
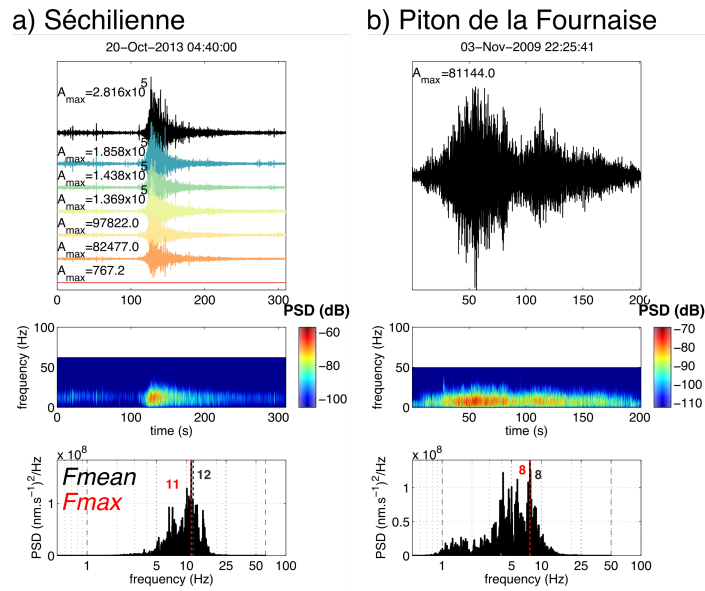
Figure 4. Dry granular flow events recorded at a) Séchilienne and b) the Piton de la Fournaise Caldera. See Fig. 2 for description of the figure.
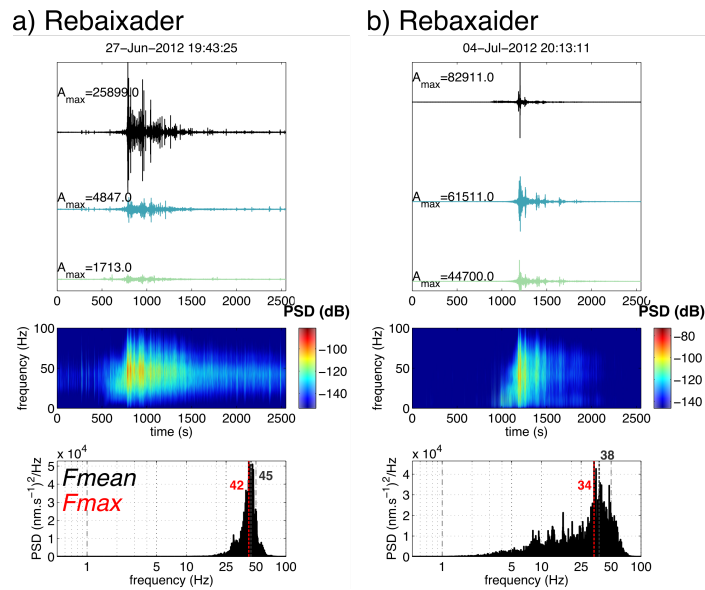
Figure 5. Wet granular flow events recorded at Rebaixader torrent (Abancó et al., 2012; Hürlimann et al., 2014; Arattano et al., 2016). See Fig. 2 for description of the figure.
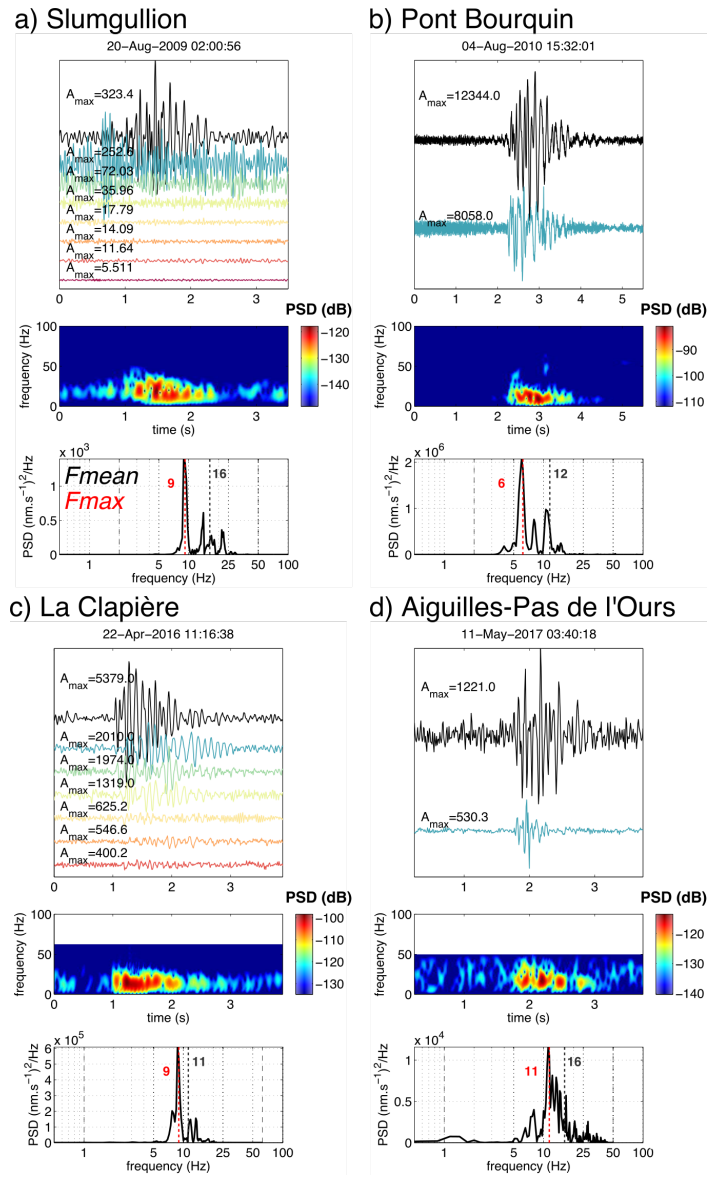
Figure 6. Low-Frequency Slopequakes recorded at the a) Slumgullion (Gomberg et al., 2011), b) Pont-Bourquin, c) La Clapière and d) Aiguilles-Pas de l'Ours slopes. See Fig. 2 for description of the figure.
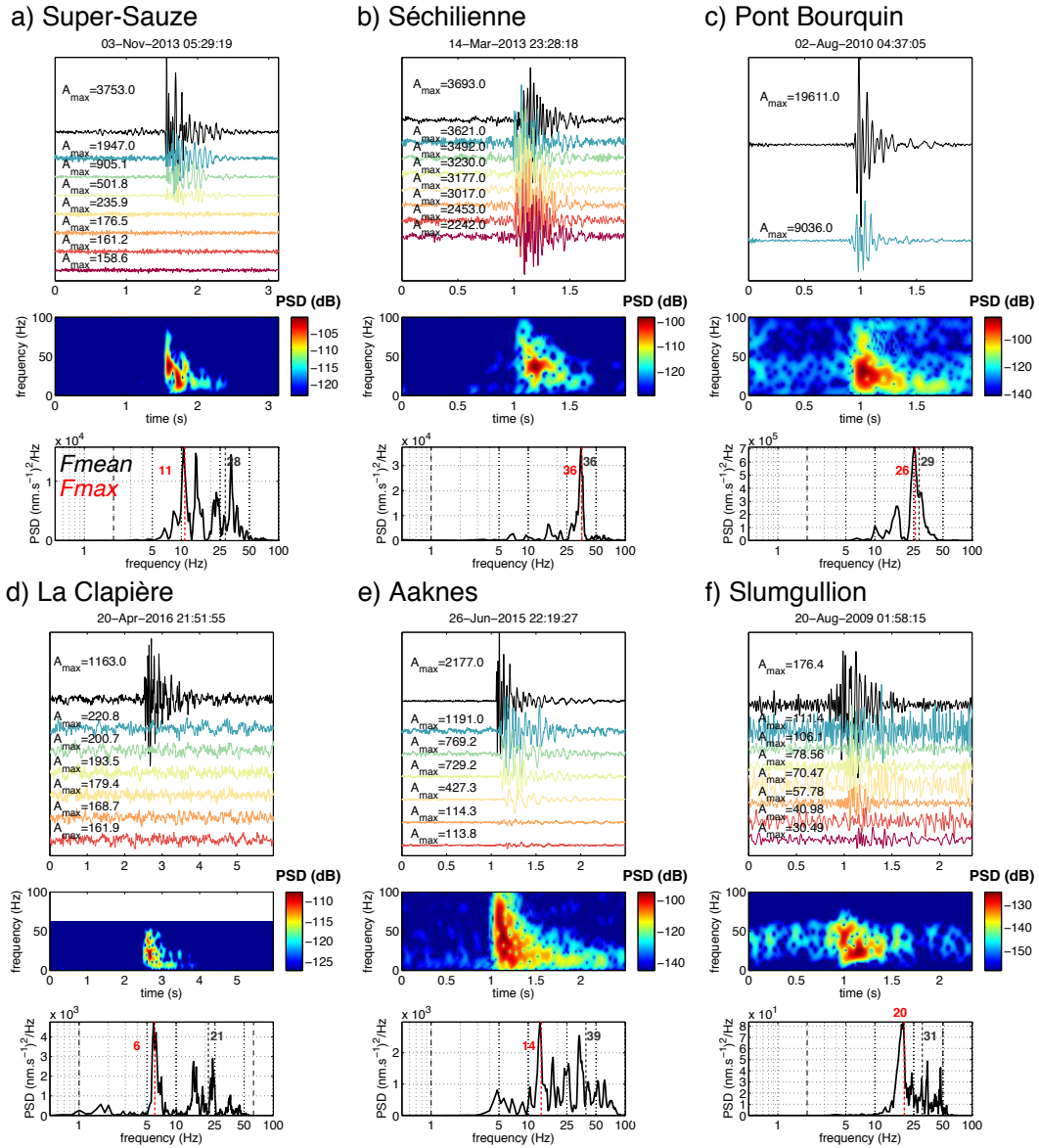
Figure 7. High-Frequency Slopequakes recorded at the a) Super-Sauze (Provost et al., 2017a), b) Séchilienne (Helmstetter et al., 2011; RE-SIF/OMIV, 2015), c) Pont-Bourquin, d) La Clapière, e) Aaknes, and f) Slumgullion (Gomberg et al., 2011) slopes. See Fig. 2 for description of the figure.
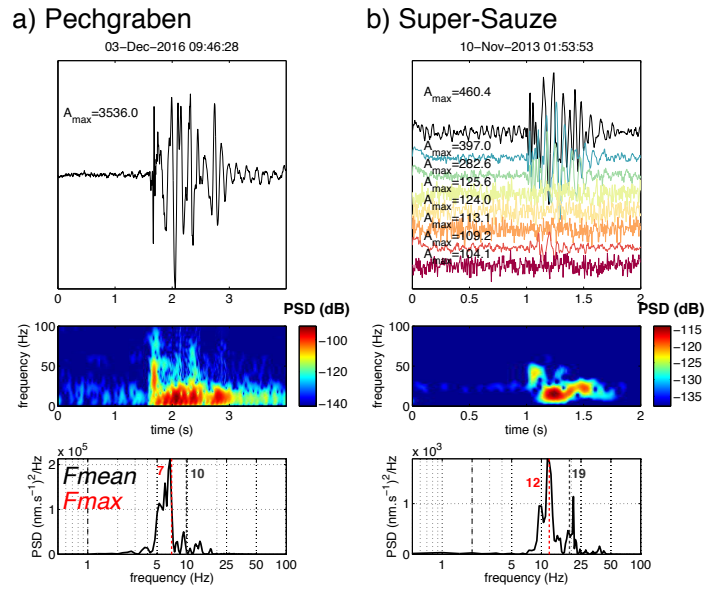
Figure 8. Hybrid-Slopequake recorded at the a) Pechgraben and b) Super-Sauze landslide. See Fig. 2 for description of the figure.
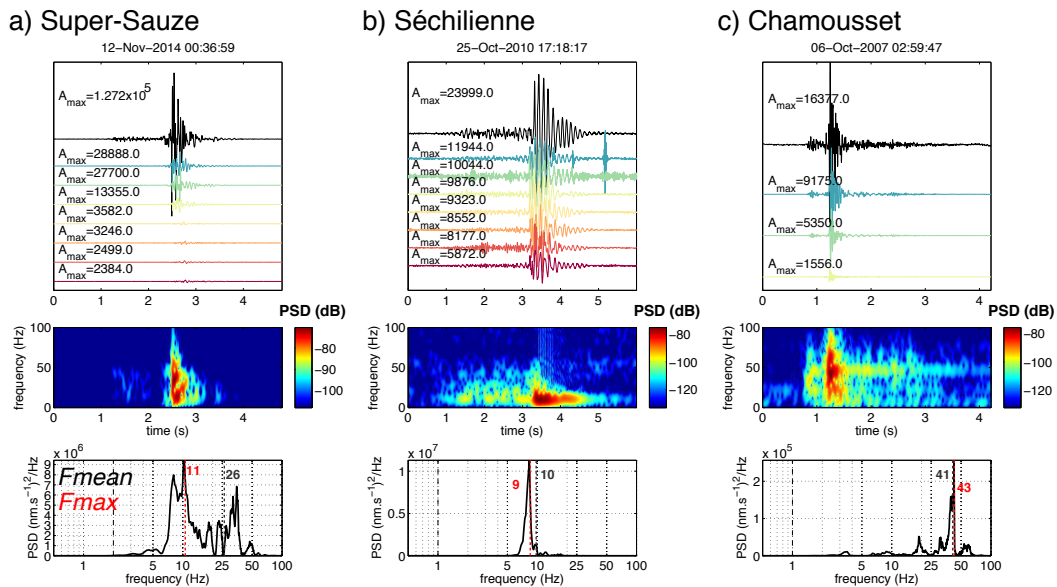
Figure 9. Examples of Slopequakes with presursory event recorded at the a) Super-Sauze, b) Séchilienne and c) Chamousset slopes. See Fig. 2 for description of the figure.
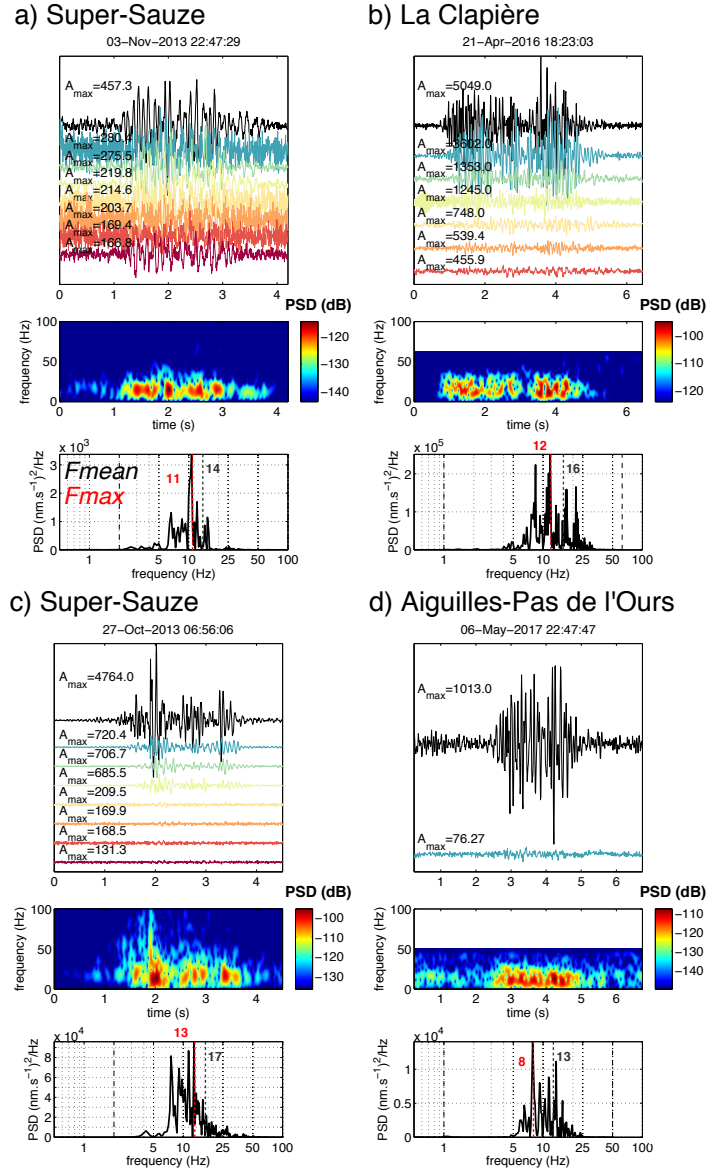
Figure 10. Examples of repetitive Slopequakes recorded at the a),c) Super-Sauze, b) La Clapière and d) Aiguilles-Pas de l'Ours slopes. See Fig. 2 for description of the figure.
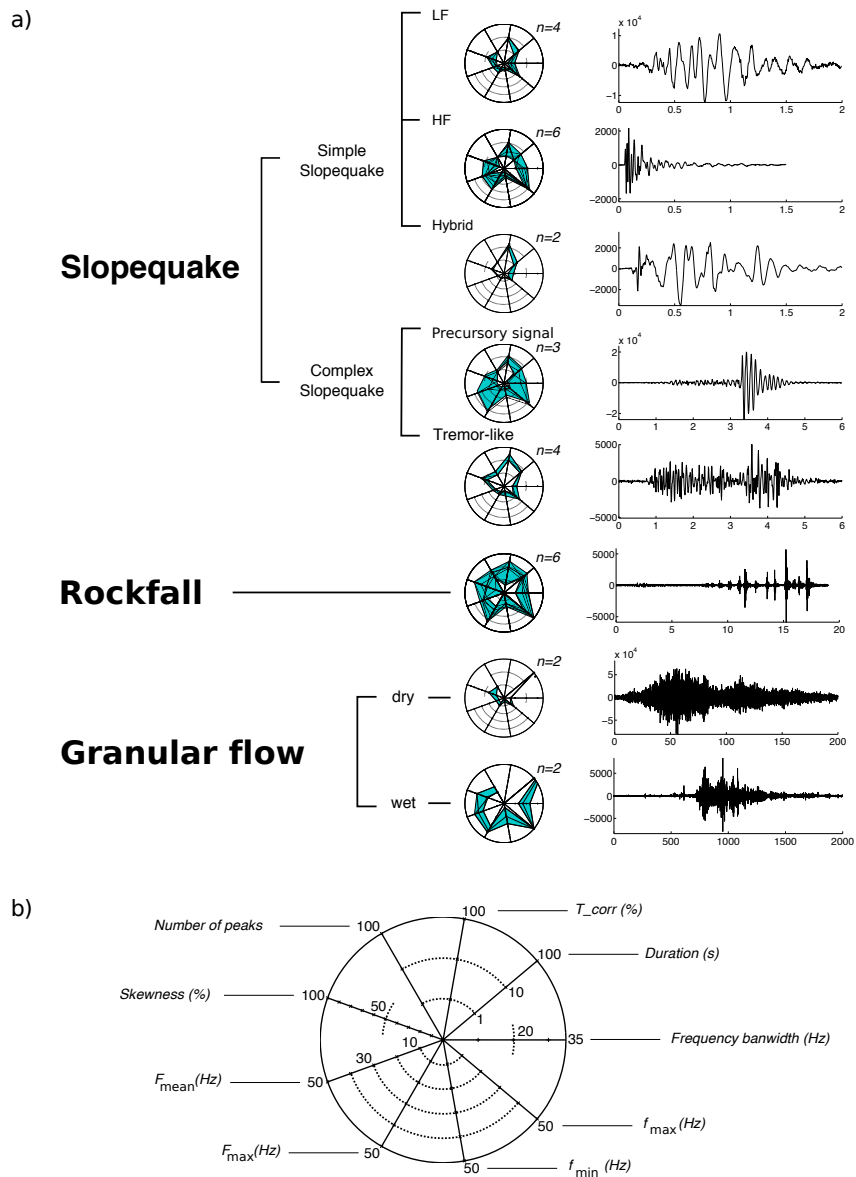
Figure 11. a) Summary of the proposed classification with plot of the attributes for the examples presented in the precedent figures and an example of waveform for each class. The convention for the attribute plot is presented in b); n being the number of seismic signals examples used to plot the feature diagram.
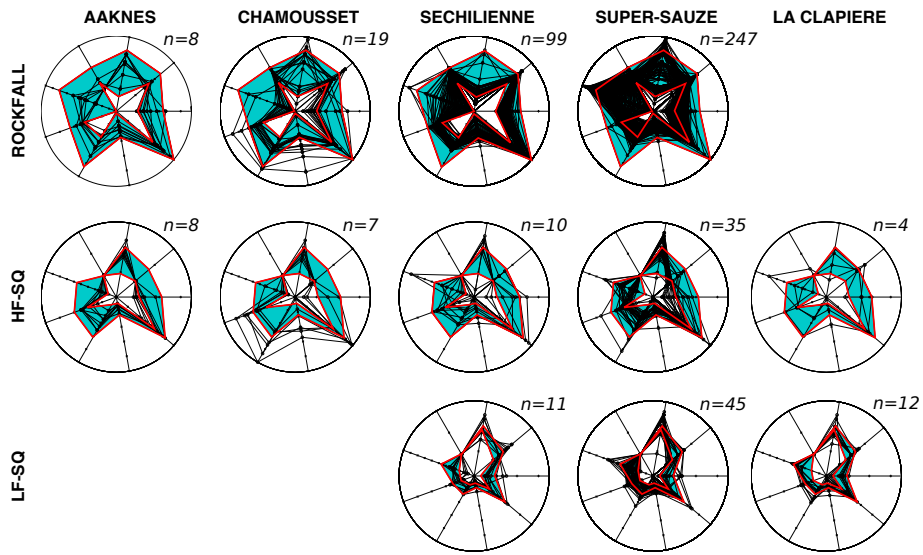
Figure 12. Variability of the signal features of classes "Rockfall", "HF-slopequake" and "LF-slopequake" for five different sites: Aaknes, Chamousset, Séchilienne, Super-Sauze and La Clapière. The axes of the star diagram are the same as in Fig. 11.
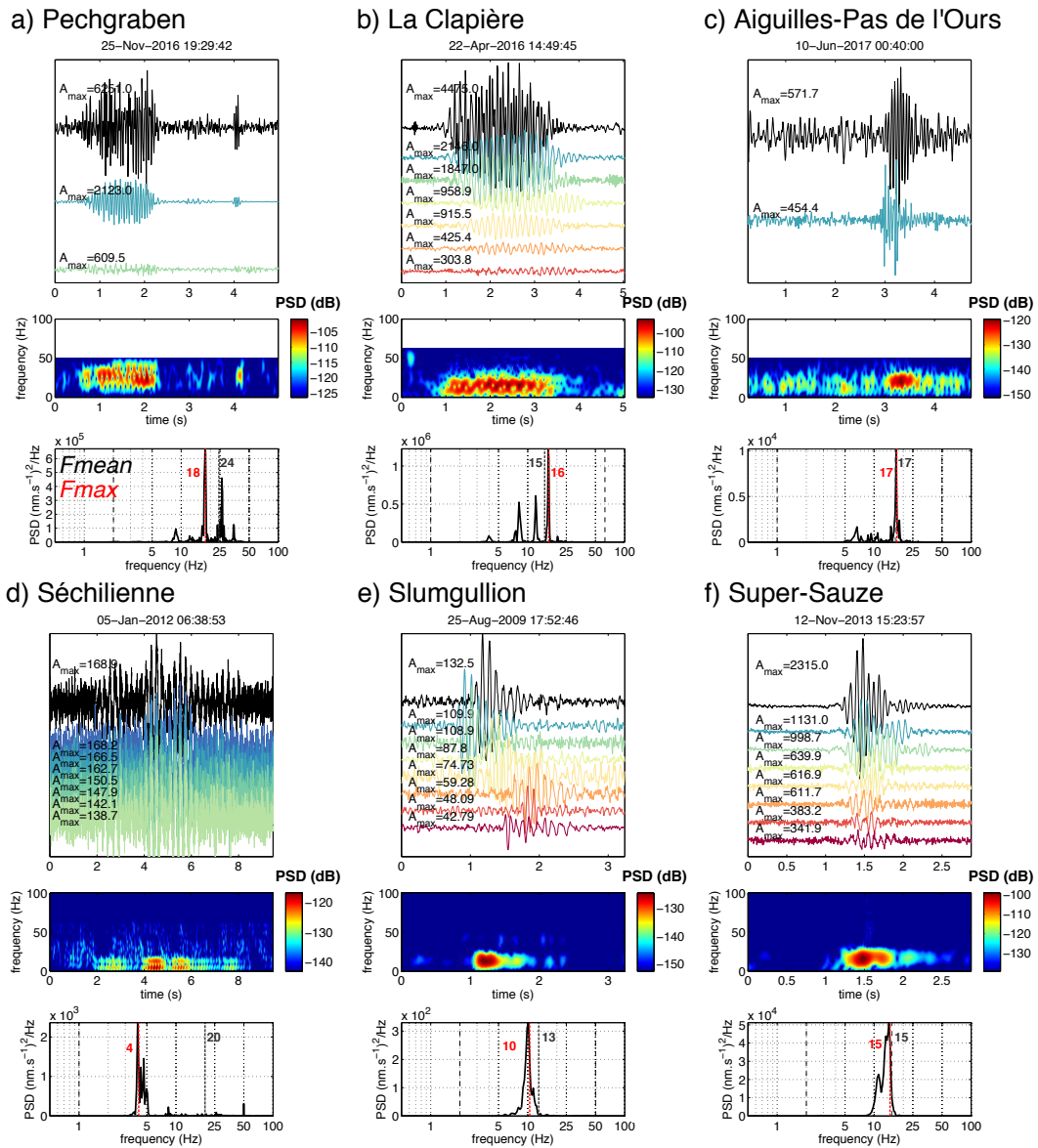
Figure 13. Examples of pure harmonic signals recorded at the a) Pechgraben, b) La Clapière and c) Aiguilles-Pas de l'Ours, d) Séchilienne, e) Slumgullion (Gomberg et al., 2011) and f) Super-Sauze slopes. See Fig. 2 for description of the figure.

Table 2. Characteristic of the seismic network for the 13 sites analyzed in the present parer. The landslide dimensions are given for the most active area of the slope instabilities (as presented in the published studies). The total number of the seismic network are given as well as its minimal and maximal inter-sensor distance and distance to the active zone. In the case a fewer number of the sensors have been investigated in the present study, we indicate the number of the sensors as well as the name of the use station in parenthesis.

Site	Sensor type	Network geom.	Number of sensors in tot.	analyzed	Inter-sensor distance min	max	Distance to the landslide min	max	Landslide dim.
Séchlienne	SP	SA	41	11 (THE)	25 m	85 m	< 50 m	< 200 m	600 m × 200 m
La Clapière	SP	SN	18	9 (CL4)	30 m	77	0 m		900 m × 700 m
Aaknes	G	SN		8	< 50 m	250 m	0 m		1 km × 1 km
Aiguilles-Pas de l'Ours	BB	SN		4	205 m	690 m	0 m	200 m	500 m × 500 m
Super-Sauze	SP	SA		8	30 m	150 m	0 m	< 100 m	800 m × 150 m
Pont Bourquin	SP	SN		2	30 m		0 m		240 m × 35 m
Pechgraben	SP	SA + SS		5	5 m	40 m	0 m		500 m × 100 m
Slumgullion	SP	D-SN		88	11 m	450 m	0 m		1 km × 500 m
Chamousset	SP	SN		7	15 m	50 m	0 m	40 m	60 m × 30 m
St. Eynard	SP	SN	4	3*	500 m	1.7 km	0 m	500 m	7 km × 300 m
Riou Bourdoux	SP,BB	SA + SS		5	50 m	200 m	20 m	30 m	length: 200 m
Piton de la Fournaise	BB	SN	10	1 (BOR)	-	-	< 50 m		1 km × 300 m
Reibaxader	G	SN		9	< 20 m	200 m	0 m		700 m × 50 m

G: Geophone (f = [0.1-10] kHz); SP: Short-Period (f = [0.1-100] Hz); BB: Broad-Band (f = [10^{-2}-100] Hz);

SN: Seismic Network; D-SN: Dense-Seismic network;

SA: Seismic Array; L-SA: Linear-Seismic Array; SS: Single Sensor;

* investigated stations: FOR, MOL, GAR.